DOI:10.14753/SE.2018.1981

Investigating the pathomechanisms of renal fibrosis in animal models – Diabetic and toxic nephropathy

PhD thesis

Csaba Imre Szalay MD

Basic Medicine Doctoral School
Semmelweis University

Supervisor:
Péter Hamar, MD, D.Sc

Official reviewers:
Csaba Kálmán Ambrus, MD, Ph.D
Attila Marcell Szász, MD, Ph.D

Head of the Final Examination Committee:
Tamás Ivanics MD, Ph.D

Members of the Final Examination Committee:
Andrea Fekete MD, Ph.D
László Wagner MD, Ph.D
Ákos Thuma, DVM, Ph.D

Budapest
2016

DOI:10.14753/SE.2018.1981

Table of contents

DOI:10.14753/SE.2018.1981

1. List of abbreviations

2D-DIGE: two-dimensional difference gel electrophoresis

ACEi: angiotensin-converting enzyme inhibitors

ACTN4: alpha-actinin-4 gene

AGE: advanced glycation end-products

AGTR1: angiotensin II receptor, type 1

ALE: advanced lipoxidation end product

AMDCC: Animal Models of Diabetic Complications Consortium

AngII: angiotensin II

ARB: angiotensin II receptor blockers

AT1R: angiotensin II type 1 receptor

BCA: bicinchoninic acid protein assay

BH: black hooded, Rowett rats

BH/c: Rowett black hooded control rats (injected with Saline)

BH/DXR: doxorubicin-injected Rowett black hooded rats

BH/DXRp: BH/DXR rat matched for urinary protein excretion

Ccl2: chemokine (C-C motif) ligand 2 or MCP-1

CD: Charles Dawley rats

CD/c: Charles Dawley control rats (injected with Saline)

CD/DXR: doxorubicin-injected CD rats

CD/DXRp: CD/DXR rat matched for urinary protein excretion

CD2AP: CD2-associated protein

CHAPS: 3-[(3-cholamidopropyl)-dimethylammonio]-1-propanesulfonate

CI: confidence interval

CKD: chronic kidney disease

COL1A1: collagen type I alpha 1

CT: cycle time

CTGF: connective tissue growth factor

Ctrl: control rat, in this case: citrate-injected Sprague Dawley rat

Cx43: connexin-43

CytP450: cytochromes P450

DAB: diaminobenzidine

DM: diabetes mellitus

DN: diabetic nephropathy

DNA-PK: DNA activated protein kinase

dsDNA: double-stranded DNA

DTT: dithiothreitol

DXR: doxorubicin

ECM: extracellular matrix

ESRD: end-stage renal disease

FP: foot process

FSGS: focal segmental glomerulosclerosis

fv: field of view

GBM: glomerular basement membrane

GFR: glomerular filtration rate

GlcNAc: N-acetyl-glucosamine

GSH: reduced glutathione

GSH-Px: glutathione peroxidase

GWAS: genome-wide association studies

H_2O_2: hydrogen peroxide

HE: hematoxylin-eosin

HIV: human immunodeficiency virus

HIVAN: HIV-associated nephritis

HNE: 4-hydroxy-2-nonenal

HClO: hypochlorous acid

IFTA: interstitial fibrosis and tubular atrophy

IHC: immunohistochemistry

LC-MS/MS: liquid chromatography tandem mass spectrometry

LDL: low density lipoprotein

LOO●: lipid peroxyl radical

LOOH: lipid hydroperoxides

MCP-1: monocyte chemotactic protein 1

MDA: malondialdehyde

MMP-9: matrix metalloproteinase 9

MPO: myeloperoxidase

mRNA: messenger ribonucleic acid

MYH9: myosin, heavy chain 9 gene

NADPH: nicotinamide-adenine dinucleotide phosphate

NGAL: neutrophil gelatinase-associated lipocalin

Ncf1: neutrophil cytosolic factor 1, neutrophil NOX-2 subunit or p47phox

NHERF2: sodium-hydrogen exchange regulatory cofactor

NO: nitric oxide

NOS: nitric oxide synthase

NOX: nicotinamide adenine dinucleotide phosphate oxidase

NPHS1: nephrosis 1 gene (encodes nephrin)

NT: nitrotyrosine

O^{2-}: superoxide

OH^{-}: hydroxyl radical

$ONOO^{-}$: peroxynitrite

OsO4: osmium tetroxide

oxLDL: oxidized low-density lipoprotein

p47phox: neutrophil cytosolic factor 1 (Ncf1), neutrophil NOX-2 subunit

p91phox: NOX-2, cytochrome b-245 beta polypeptide, neutrophil NOX-2 subunit

PAS: periodic acid–Schiff

PBS: phosphate-buffered saline solution

PC: podocalyxin

p-ezrin: phosphorylated ezrin

PKC: protein kinase C

PUFA: polyunsaturated fatty acids

PVDF: polyvinylidene difluoride

RAAS: renin-angiotensin-aldosterone system

RAGE: receptor of advanced glycation end-products

RCF: relative centrifugal force

RNS: reactive nitrogen species

ROS: reactive oxygen species

RT-qPCR: reverse transcription - quantitative polymerase chain reaction

SCID: severe combined immunodeficiency

SD: Sprague Dawley rats

SDS: sodium dodecyl sulfate

SDS-PAGE: sodium dodecyl sulfate-polyacrylamide gel electrophoresis

sGC: soluble guanylyl cyclase

SHR: spontaneously hypertensive rats

SNP: single nucleotide polymorphism

SNX: subtotal nephrectomy

SOD: superoxide dismutase

SPF: specific pathogen free

STZ: streptozotocin

TBM: tubular basement membrane

TBS: Tris-buffered saline

TBS-Tween: Tris-buffered saline supplemented with 0.1% Tween-20

TEM CCD: transmission electron microscopy charge-coupled device

TGFB1: transforming growth factor beta 1 gene

TGF-β1: transforming growth factor β1

TNF-α: tumor necrosis factor α

VEGF-A: vascular endothelial growth factor A

WKY: Wistar-Kyoto rat

DOI:10.14753/SE.2018.1981

2. Introduction

Chronic kidney disease (CKD) is a progressive and irreversible loss of kidney function over a longer period of time. CKD slowly progresses to end-stage renal disease (ESRD), independently from the primary insult. ESRD is a life threatening condition, which requires renal replacement therapy in the forms of dialysis or kidney transplantation. For this reason CKD is a major healthcare problem with a prevalence of 7% in Europe (1), and over 10% in the US according to the Centers for Disease Control and Prevention (2).

The most common cause of CKD is diabetes mellitus (DM) (3). The risk factors for developing CKD include high blood pressure, cardiovascular disease, obesity, high cholesterol, lupus, and a family history of CKD. The primary diagnosis for ESRD in the USA in 2012 were diabetes (53,2%), hypertension (34,6%), glomerulonephritis (9,5%) and cystic kidney (2,7%) according to the US Renal Data System 2015 Annual Data Report (4).The clinical presentation of CKD varies widely among patients with the same initial disease (5,6). The severity of symptoms and the rate of CKD progression are influenced by age, gender (7,8) and numerous pieces of evidence support a role for genetic background in progression (9-11). The pathologic manifestation of CKD is a loss of glomerular filtration, proteinuria and renal fibrosis, characterized by an exaggerated wound-healing process with the production of renal scar tissue (12). Over the last decade significant progress has been made in the understanding of the molecular mechanisms behind CKD, however no specific treatment is available that would be able to arrest or reverse the progression (13).

Glomerular injury is a key step in the development of many forms of CKD. The role of podocytes in glomerular injury is under intense investigation. The podocyte is a highly complex cell involved in maintaining glomerular structure and function.(14,15). The podocyte foot processes form the slit diaphragm, an important part of the glomerular filtration barrier (Figure 1). The three main forms of podocyte injury are foot process effacement, dedifferentiation and apoptosis (12). Targeting toxins to the podocyte using transgenic expression of the human diphtheria toxin receptor in rat podocytes appears to be sufficient for inducing focal segmental glomerular sclerosis (FSGS) like lesions with albuminuria in rodents (15,16). For these reasons our workgroup performed several

DOI:10.14753/SE.2018.1981

experiments to uncover new mechanisms behind the glomerular changes in CKD focusing on the role of podocytes (17,18).

In the following sections I would like to introduce three aspects of CKD, which were investigated to some extent by our workgroup: 1. Glomerular injury as a result of diabetes mellitus, 2. The role of oxidative stress in CKD, 3. The role of genetic background in the progression of CKD.

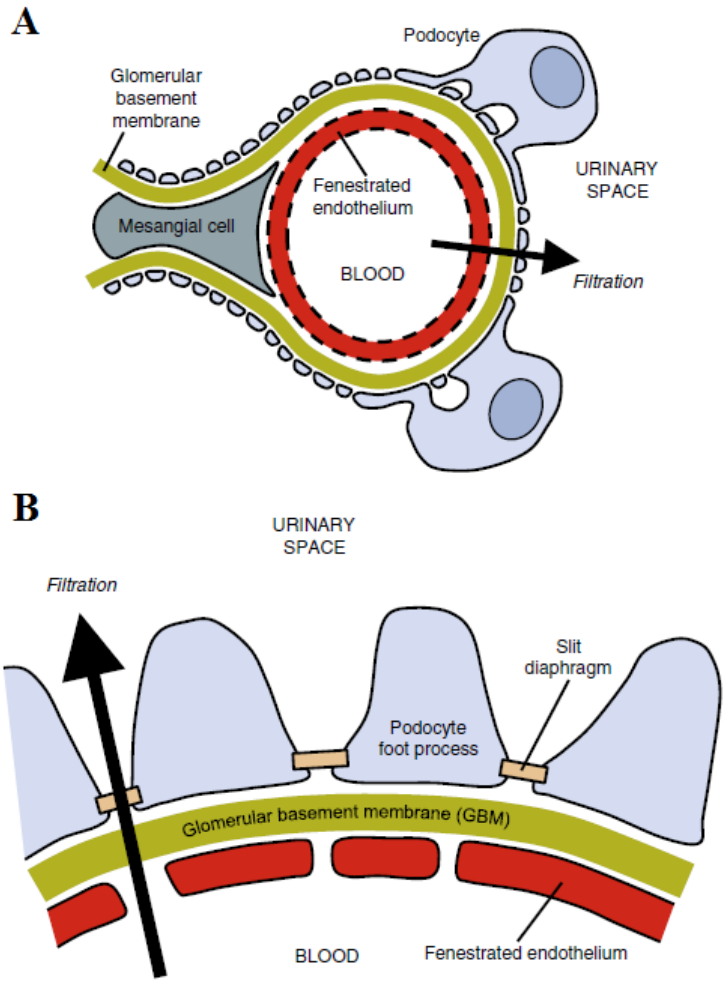

Figure 1: Glomerular structure:

A: Schematic representation of a glomerular capillary loop showing the arrangement of podocytes, mesangial cells and of the endothelium. B: Enlarged view of the glomerular filtration barrier: fenestrated endothelium, glomerular basement membrane and podocyte foot processes with their filtration slits.

From: Leeuwis JW. et al. 2010 (12)

2.1. Diabetic nephropathy:

Diabetic nephropathy (DN) is a serious complication of diabetes mellitus occurring in approximately 20–30% of patients with diabetes mellitus (19,20). The annual incidence of this disease has more than doubled in the past decade, and it accounts for almost 50% of all ESRD (21). The earliest symptom of DN is microalbuminuria that progresses into nephrotic syndrome with high blood pressure and progressively impaired kidney function, which manifests as a decrease in glomerular filtration rate (GFR). The gold standard in the diagnosis of DN is kidney biopsy; however its use is limited by its invasiveness (22). The histological hallmarks of DN seen with light microscopy are thickening of the glomerular (GBM) and tubular (TBM) basement membranes, mesangial expansion (diffuse and later nodular: Kimmel-Wilson lesions), segmental glomerulosclerosis (especially at the tubular outlet: tip lesion), hyalinosis of afferent and efferent arterioles and microaneurysms of glomerular capillaries. The glomerular changes are often followed by tubular atrophy and interstitial fibrosis (Figure 2). Diffuse linear accentuation of the glomerular and tubular basement membranes, nonspecific segmental staining of the glomeruli is often seen with immunofluorescence microscopy. The earliest changes in GBM thickness can be detected with electron microscopy. Podocyte foot process effacement also occurs during the later stages of the disease (23).

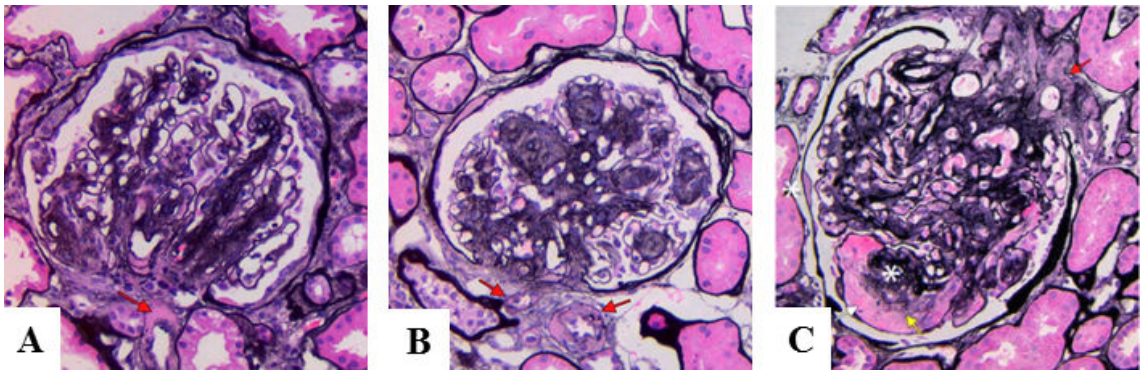

Figure 2: Histological features of Diabetic nephropathy:

A: DN with diffuse mesangial expansion and arteriolar hyalinosis (red arrow).

B: DN with nodular mesangial expansion (Kimmelstiel-Wilson nodules) and concomitant hyalinosis of afferent and efferent arterioles (red arrows; Jones silver stain).

C: Kimmelstiel-Wilson nodule (upper asterisk), with adjacent mesangiolysis (yellow arrow) and a microaneurysm (white arrow), with prominent arteriolar hyalinosis (red arrow). There is a capsular drop (lower asterisk) on Bowman capsule (Jones silver stain). From: Najafian B. et al. (2015) (20)

The pathomechanisms of DN are complex. Recent studies indicate that podocyte dysfunction plays an important role (24) in the early stages of DN. Elevated systemic blood pressure increases the intraglomerular pressure, leading to glomerular hyperfiltration (19,25). Excess blood glucose binds to amino groups of peptides to form advanced glycation end products (AGE) (26). AGE can induce an increased production of reactive oxygen species (ROS) in the glomerulus (27). AGEs also bind to the proteins of the extracellular matrix (ECM) inhibiting its degradation (19). Podocytes express receptors for AGEs (RAGE) on their cellular surface, thus AGE binding can induce TGF-β production in podocytes (28). TGF-β is a master regulator of fibrotic processes, it has both profibrotic and apoptotic effects, leading to loss of podocytes and to glomerulosclerosis (29). Angiotensin II (AngII) decreases nephrin expression and induces proteinuria by directly affecting the podocytes through the AngII type 1 receptor (AT1R) (29),(30,31).

Besides the elevated serum glucose levels, insufficient insulin secretion or insulin resistance also contribute to the decrease of glomerular function. Recent studies suggest that insulin signaling in podocytes is essential to maintain normal glomerular ultrafiltration. Deletion of the insulin receptor specifically from podocytes leads to albuminuria and histological changes resembling DN even under normoglycemic conditions (32). In response to insulin, podocytes take up glucose via glucose transporters GLUT4 (33). Treatment of cultured podocytes with insulin induces rapid remodeling of the actin cytoskeleton (32). In many types of glomerular diseases the integrity of the actin cytoskeleton is altered in podocytes, indicating that proper organization and regulation of the actin cytoskeleton are essential for podocyte structure and function (34). Proteins involved in actin organization can be potential therapeutic targets in the treatment of glomerular diseases, including DN.

Ezrin is an important regulator of actin dynamics, linking membrane proteins to the underlying actin cytoskeleton (35-37) with its interaction partner sodium-hydrogen exchange regulatory cofactor (NHERF2). Ezrin and NHERF2 are expressed in podocytes, where they connect the cell surface sialoprotein podocalyxin to actin (38-40). Also the N-terminal fragment of ezrin has been shown to bind to AGEs in the kidneys of diabetic rats (41). For these reasons ezrin may play an important role in podocyte injury in DN.

2.2. The role of oxidative stress in CKD

Oxidative stress or oxidant-derived tissue injury results from an overproduction of reactive oxygen/nitrogen species or impairment in the cellular antioxidant enzyme activities, leading to oxidation of macromolecules such as proteins, carbohydrates, lipids, and DNA (42). Among the reactive oxygen species (ROS) that drive oxidative stress, the most important are superoxide anion (O^{2-}) and hydrogen peroxide (H_2O_2).

O^{2-}, which are by-products of the respiratory chain, and are produced during normal cellular function (43). O^{2-} production by NADPH oxidase (NOX) is important for the anti-pathogen activity of the inflammatory cells. O^{2-} is rapidly converted into H_2O_2 by superoxide dismutase. H_2O_2 can be converted into H_2O by catalase, peroxiredoxins, or glutathione peroxidase (GSH-Px). On the other hand, H_2O_2 can be metabolized by myeloperoxidase to form hypochlorous acid (HOCl) (44), and the reaction of H_2O_2 with Fe^{2+} forms the highly reactive hydroxyl radical (OH^-). These molecules have strong anti-pathogen activity; however if the antioxidant mechanisms are insufficient, these molecules may cause severe oxidative damage to the cells of the body (45). For this reason increased NOX activity in response to proinflammatory mediators contributes to increased ROS formation and oxidative stress (43).

Peroxynitrite ($ONOO^-$) is produced by the interaction of superoxide (O^{2-}) and nitrogen monoxide (NO). This reaction can be seen as NO scavenges O^{2-}; however, the formed $ONOO^-$ peroxidizes macromolecules such as lipids and proteins including LDL, in which peroxidation of tyrosine residues leads to nitrotyrosine (NT) formation (44). The prolonged peroxidation of macromolecules by reactive nitrogen species is called nitrative stress. NO is also an important intracellular messenger causing vasodilatation by activating the soluble guanylyl cyclase (sGC). Thus, increased formation of $ONOO^-$ decreases the bioavailability of NO and thus, attenuates its vasodilatory effects (45).

Polyunsaturated fatty acids (PUFA) undergo peroxidation in the presence of free radicals, leading to the production of lipid peroxyl radicals ($LOO^{\bullet}$) generating further lipid hydroperoxides (LOOH). LOOH molecules are unstable, and promote the formation of reactive aldehydes, such as malondialdehyde (MDA) and 4-hydroxynonenal (HNE) (45). Plasma MDA level and tissue HNE content are widely

used markers of lipid peroxidation (46). Oxidative modification of low-density lipoprotein (oxLDL) makes these particles cytotoxic to vascular endothelial cells and promotes atherogenesis (47). Kalyanaraman B. and Griffith O. created a schematic representation of the most important pathways of free radical production (Figure 3).

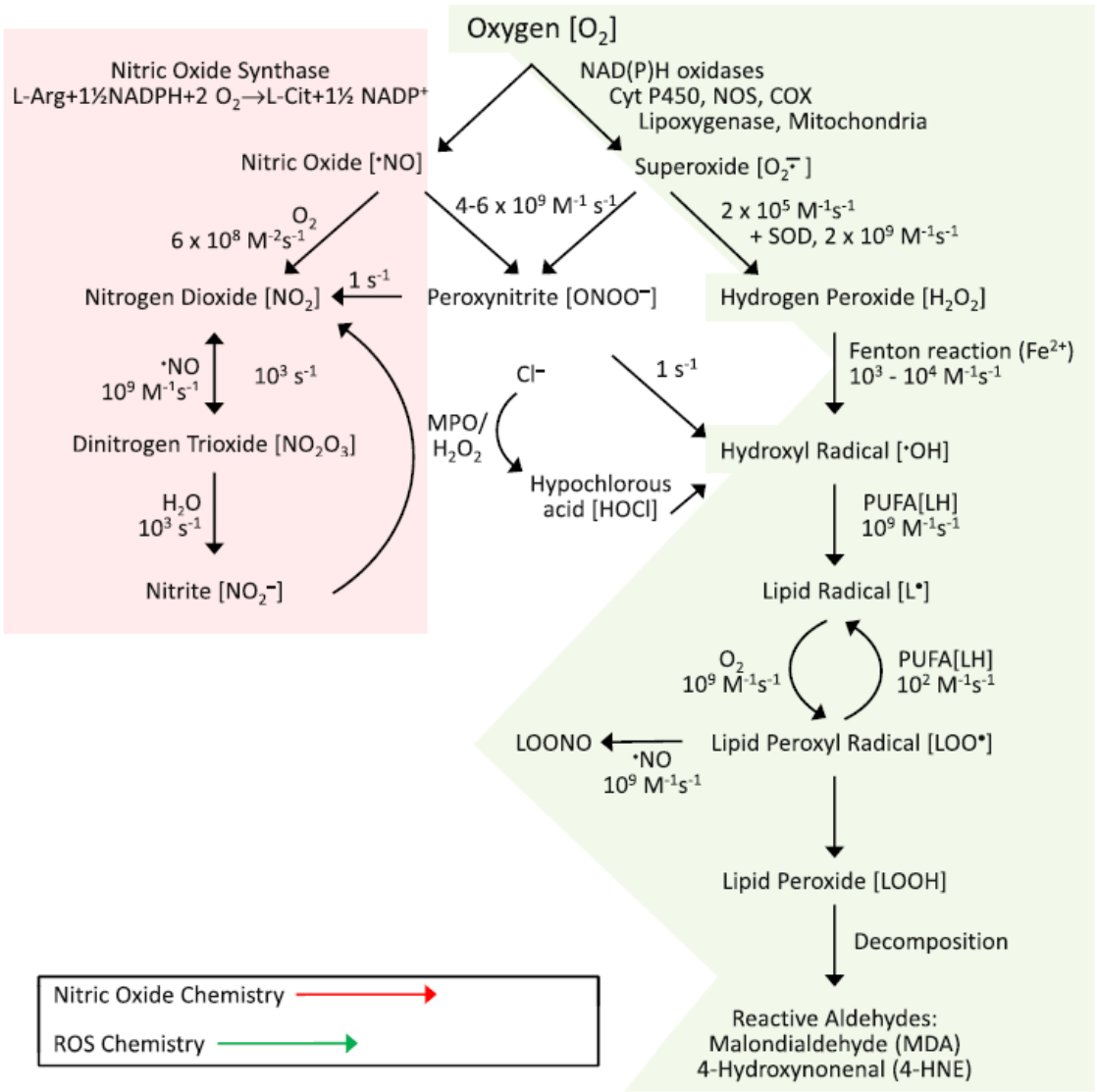

Figure 3: Generation of reactive oxygen and nitrogen species

From: Kalyanaraman B (2013) (45)

Advanced glycation end products (AGE) play an important role in the development of diabetic nephropathy, but also in CKD in general. AGE formation has been described originally as a non-enzymatic reaction between proteins and glucose in the Maillard reaction (48). However AGEs also can be formed during oxidative stress by lipid-

derived intermediates (resulting in advanced lipoxidation end-products (ALE)) and reactive carbonyl compounds (carbonyl stress) (48,49).

As discussed previously, AGEs can bind to its receptors (RAGE) on the surface of different cells. Binding of AGE to RAGE results in elevated ROS production via a TGF-β1-mediated pathway in podocytes. This mechanism of ROS production is relevant in diabetic nephropathy because of the hyperglycemia-induced AGE production. However, in other forms of CKD the excretion of AGEs decreases through the declined GFR, and it contributes to the RAGE and TGF-β1-mediated ROS production, creating a vicious circle (26).

ROS have a short half-life and can be metabolized by antioxidant defense mechanisms. These mechanisms include enzymes, like superoxide dismutase (SOD), catalase, and GSH-Px. Other, non-enzymatic substances, like reduced glutathione (GSH), vitamins A, C and E, albumin, ferritin, transferrin, and uric acid as well as prevention of magnesium and zinc deficiency are also required for optimal antioxidant defense (43,47). Certain genetic polymorphisms in glutathione S-transferase are more frequent in ESRD, thus these polymorphisms can modulate the degree of oxidative stress in patients with CKD (50). Angiotensin-converting enzyme inhibitors (ACEi), angiotensin receptor blockers (ARB), statins, vitamin E and Vitamin D supplementation can be effective against oxidative stress in CKD (51,52).

Oxidative stress occurs early in the development of CKD. Massive proteinuria in nephrotic syndrome causes oxidative stress and interstitial inflammation. Sustained interstitial inflammation contributes to renal injury in multiple ways. As it was mentioned previously, increased NOX activity, by the production of potent free radicals, like O^{2-} and subsequent formation of $ONOO^-$, OH^- and HOCl combined with the insufficient antioxidant mechanisms in CKD leads to oxidative damage of the interstitial cells (53). Uremic toxins also contribute to AGE and ALE production, while the detoxification of these molecules is attenuated (48,54). Ligand binding of RAGE also leads to increased ROS production. High ROS levels in the renal medulla block the vasodilatory effects of NO, thereby decreasing the blood flow and leading to medullary hypoxia (49),(55). Activation of the renin-angiotensin-aldosterone system (RAAS) in

hypertensive patients with impaired renal function leads to increased ROS production via the activation of different NOX isoenzymes (44,47). The NOX isoforms expressed in the kidney cortex are NOX1, NOX2 and NOX4. Both NOX2 and NOX4 can be upregulated by angiotensin II, and NOX2 activation requires the recruitment of its cytosolic subunits (p47phox, p67phox, p40phox and Rac1) (56).

Although a great variety of markers are available for estimating oxidative stress in experimental investigations, there is no gold standard for measuring or monitoring oxidative stress in the clinical practice (57). In our experiments we used HNE as a marker of lipid peroxidation and nitrotyrosine (NT) to estimate nitrative stress caused by reactive nitrogen species (18).

2.3. The role of genetic background in CKD:

The rate of progression of CKD varies between individuals with the same initial disease. Growing evidence suggests a strong role for genetic background in the progression of CKD (58,59). It has been observed that close family members with hypertension develop similar degree of renal injury. The hypothesis that this phenomenon is caused by hereditary factors was further supported by performing linkage studies in segregating populations of spontaneously hypertensive rats (60). Racial differences also influence the progression of CKD. People with African ancestry have significantly higher risk for human immunodeficiency virus (HIV)-associated nephropathy (11). Black Americans are more susceptible for developing hypertension-induced renal injury or diabetic nephropathy (61,62). The prevalence of end-stage renal disease is significantly higher among Indigenous Australians as well. The key factors suspected behind this tendency are fewer nephron count and renin-angiotensin system gene polymorphisms (63).

Familial clustering and genome-wide association studies (GWAS) identified several gene mutations responsible for the development of CKD. Certain mutations of the NPHS1 Nephrosis 1 gene (NPHS1) play an important role in the development of the Finnish type congenital nephrotic syndrome that has an autosomal-recessive inheritance (64). NPHS1 gene encodes nephrin, a protein expressed on the podocyte foot process

surface, which is an important element of the slit diaphragm. Podocin interacts with nephrin and cluster of differentiation marker-2 (CD2)-associated protein (CD2AP) within lipid rafts (65). Altered expression of these proteins can also lead to the development of nephrotic syndrome. Kaplan and his coworkers found that certain mutations in the alpha-actinin-4 encoding gene (ACTN4) cause or increase susceptibility to FSGS. The product of ACTN4 gene is alpha-actinin 4, an actin-filament crosslinking protein, which is highly expressed in the foot processes of podocytes. The mutations increase the binding of alpha-actinin-4 to actin filaments causing defects in the regulation of the actin cytoskeleton (10). These findings further support the importance of the functional and structural integrity of the podocyte cytoskeleton and the slit diaphragm in maintaining glomerular function. Inherited defects of podocyte-related genes are major risk factors for many forms of kidney failure (11). According to genome-wide admixture mapping studies the myosin heavy chain 9 encoding gene (MYH9) was suggested to play a role in the susceptibility to develop CKD in African–Americans. MYH9 encodes the non-muscle myosin heavy chain type II isoform A, which is highly expressed in the podocyte foot processes and also in the renal tubules (59).

Certain gene polymorphisms may also increase susceptibility for developing CKD. (58,66). A prospective population-based study of CKD risk led to the conclusion that polymorphism of the angiotensinogen promoter G(-6) can increase the probability of developing CKD, but only in the presence of hypertension (67). A retrospective study of single nucleotide polymorphisms (SNPs) in patients who received kidney transplants demonstrated that certain polymorphisms in the genes encoding transforming growth factor beta 1 (TGF-β1), angiotensin II receptor type 1 (AGTR1) and vascular endothelial growth factor A (VEGF-A) are associated with susceptibility or protection against chronic renal allograft dysfunction (68). Some genes encoding proteins involved in vasomotor and inflammatory function are also suspected in the development of CKD according to a meta-analysis (69). Additional gene loci are remaining to be identified to fully understand the genetic variance in renal function.

Animal models of CKD already provided useful data to understand the mechanisms behind the inherited differences in the progression of CKD. Fitzgibbon and his coworkers provided evidence that inherited differences in the response to the action of aldosterone may contribute to individual differences in CKD progression. Wistar-Furth rats, known to be resistant to actions of mineralocorticoids, developed milder albuminuria and glomerular damage compared to Wistar rats in a subtotal nephrectomy model of CKD (7). The C57BL/6 mice are also relatively resistant to glomerulosclerosis compared to other mouse strains in different CKD models. The nature of this resistance has been extensively investigated. Differences in the activity of RAAS were demonstrated to contribute to this phenomenon, because administering angiotensin II could overcome the resistance of C57BL/6 mice to develop CKD (70,71). However, other mechanisms of inherited resistance for developing CKD were proposed based on experimental data from the Doxorubicin-nephropathy model in C57BL/6 mice. Compared with the sensitive BALB/c mice, the immune responses of the C57BL/6 mice were more polarized towards the Th1 axis, producing greater amounts of IL-12 and IFN-γ. On the other hand the immune responses of the BALB/c mice were more polarized towards the Th2 axis, with elevated IL-4 production compared to the C57BL/6 mice (72). These results further support the theory that differences in inflammatory gene expression contribute to susceptibility to renal injury (69). Genetically modified rodent strains can be very useful tools to study not just the pathomechanisms of CKD, but also to test novel therapeutic strategies (73).

In the following I would like to introduce two widely used animal models for CKD, which were used by our workgroups during the experiments of the present thesis:

2.4. The streptozotocin (STZ)-induced diabetic nephropathy (DN) model

Streptozotocin-induced diabetes is the most widely used rodent model to study DN. STZ is an analogue of N-acetyl glucosamine (GlcNAc), which is transported into pancreatic β-cells by the glucose transporter GLUT-2, and causes cell toxicity leading to loss of beta-cells with consequent absolute insulin deficiency (74). Rodents develop hyperglycemia, followed by albuminuria, elevated serum creatinine and histological lesions associated with diabetic nephropathy, depending on strain sensitivity (75). There

is potential collateral tissue toxicity for STZ that makes it complicated to interpret the cause of kidney injury in this type of DN model (76). Low-dose (40-50 mg/kg) STZ injections are preferred to minimize nonspecific cytotoxicity and develop a diabetes specific nephropathy (77,78). In order to increase the β-cell toxicity of low-dose STZ, animals are often starved before STZ injection. STZ can be administered intravenously, usually via the tail vein. Intraperitoneal administration is also possible, but the dosing is less accurate as it depends on peritoneal absorption and a higher dose of STZ is needed (75,79). Sprague-Dawley (SD), Wistar-Kyoto (WKY) or spontaneously hypertensive (SHR) rats are frequently used strains for STZ-induced diabetes but the dose depends on the strain used.

The Animal Models of Diabetic Complications Consortium (AMDCC) published validation criteria for rodent models of DN. These are: >50% decrease in renal function, >10-fold increase in albuminuria, pathological features including advanced mesangial matrix expansion (with or without nodules), thickening of the GBM, arteriolar hyalinosis and tubulointerstitial fibrosis (80). Although the renal histological changes seen in STZ-induced DN in rats closely resemble those in humans (3), this model does not completely satisfy the criteria set by the nephropathy subcommittee of AMDCC (81). Streptozotocin causes hyperglycemia and severe albuminuria in sensitive rodent strains; however minimal evidence of renal scarring is present. In order to cause more severe glomerulosclerosis and tubulointerstitial fibrosis, injection with STZ can be combined with uninephrectomy, or spontaneously hypertensive (SHR) rats can be used (75). Rodent kidneys in these combined models show histological changes similar to a more advanced stage of human DN, but arteriolar hyalinosis, or significant decline in renal function cannot be observed (81). These features make the STZ-induced DN model more suitable to study the early changes in glomerular function associated with DN.

2.5. The Doxorubicin nephropathy model

The anthracycline derivative chemotherapeutic drug, doxorubicin (Adriamycin, DXR) is widely used to induce proteinuric nephropathy leading to renal fibrosis as a model of a toxic renal injury-induced chronic renal fibrosis in rodents (72). Although it is generally accepted that an initial injury to podocytes induces proteinuria, the exact

pathomechanism of the DXR-induced nephropathy is poorly understood (82). Doxorubicin causes direct toxic damage to the glomerulus, with subsequent tubulointerstitial injury, which can be avoided by clipping the renal artery during the injection (83). Increased O_2^- and OH^- radical formation leads to AGE formation, AGE-RAGE interaction and lipid peroxidation. One-electron reduction of the quinone group in the C ring of DXR results in the formation of a DXR semiquinone radical. This molecule undergoes redox-cycling in the presence of oxygen, which leads to the production of O_2^-; however DXR is not consumed during the reaction. This phenomenon is called futile redox-cycling process. Interaction between the released O_2^- and mitochondrial iron containing proteins results in the generation of hydroxyl radicals (45,84). NOX and p44/p42 MAP kinase signaling also play a role in the glomerular injury caused by DXR (85,86).
DXR has other effects, like causing alterations in DNA structure. DXR-injection, especially with multiple shots, causes myelotoxicity, hepatotoxicity and cardiomyopathy (72). The cardiac effects of multiple DXR injections are used as a rodent cardiomyopathy model (87,88).

The optimal DXR dose for inducing nephropathy depends on rodent species, strain, gender and age. The intravenous route for DXR injection is preferable via the tail vein. Intraperitoneal route is also acceptable, however the absorption of the drug through the peritoneal membrane is variable (89). Glomerular injury can be achieved with single or multiple injections, but multiple injections may cause cardiac injury (87,88). DXR dissolves in saline, and similarly to STZ it is light sensitive.

DXR causes direct toxic damage to most glomerular cells, however primary and most investigated toxicity is podocyte damage, leading to the loss of nephrin (90) and consequent proteinuria (91). Ultrastructural examination of the podocytes demonstrated the first signs of injury in the foot processes (FP) on the 3rd day after DXR injection. By day 7 FPs become broad and swollen. On day 14 some of the FPs are lost, the rest becomes broader. The podocyte cell bodies also swell, and cytoplasmic vesicles and inclusions can be detected. On day 28 FP fusion and effacement are present with more evident podocyte alterations (92). Significant proteinuria can be detected around two

weeks after DXR injection. DXR administration to rats also leads to severe tubulointerstitial inflammation with marked infiltration by T and B lymphocytes and macrophages. The intensity of inflammation correlated with the DXR-induced renal damage, and suppression of monocyte chemotactic protein 1 (MCP-1), $p47^{phox}$, $p91^{phox}$, TNF-α and IL-1β-related pro-inflammatory pathways affected the severity of renal damage in this model (93-95).

There are difficulties in using this model, because DXR has a narrow "therapeutic" window and individual susceptibility as well as significant batch variability makes dosing more difficult. For these reasons dose finding experiments are recommended. Despite these technical difficulties, the DXR- nephropathy model is a widely used and favored model for CKD, because it is highly reproducible. Renal injury is severe but with appropriate dosing, acute mortality is low (<5%). The timing of the functional and structural changes is predictable, which makes this model ideal to test interventions to slow the progression and to prevent renal damage (72).

DOI:10.14753/SE.2018.1981

3. Objectives

We investigated the pathomechanisms involved in the development of CKD and renal fibrosis using two different animal models of renal injury.

In the diabetic nephropathy study we investigated early molecular changes in the development of DN (17). The objectives of these experiments were the following:

1. To explore the changes in the protein expression profile of glomeruli at an early stage of the STZ-induced diabetes in rats.
2. To identify glomerular proteins with altered expression compared to healthy controls.
3. To identify the role of these proteins in the development of diabetic nephropathy.

The toxic nephropathy study was a continuation of an earlier study of our group. Rowett, black hooded (BH) rats were resistant to renal fibrosis induced by subtotal nephrectomy plus salt and protein loading (96). We conducted experiments to identify the possible mechanisms behind this resistance. The objectives of the toxic nephropathy study were: We used the Doxorubicin nephropathy model for our investigations (18).

1. To investigate whether the Rowett rats develop less severe renal injury than control CD rats in a model of chronic renal fibrosis initiated by toxic podocyte injury.
2. What sort of structural changes develop in the kidney of Rowett rats after direct toxic damage to the podocytes.
3. Since the earlier study suggested that less oxidative stress may be responsible for this resistance of the Rowett rats to renal fibrosis, we analyzed factors of oxidative and nitrative stress in the kidney of Rowett rats after renal injury.

4. Methods

4.1. Ethics Statement

Humane endpoints were used to minimize suffering in survival studies. Animals were observed and weighed every morning after potentially lethal interventions. If clinical signs of distress were recognized the animals were euthanized by bleeding from the aorta under ketamine + xylazine (CP-Ketamine 10%, CP-Xylazine 2%, CP-Pharma, Burgdorf, Germany) anesthesia performed by a trained personnel. Uremic signs or body weight loss > 40% of the initial body-weight was an indication for euthanasia. Clinical signs of uremia included reduced locomotion, piloerection, body weight loss or dyspnea. Sacrifice for organ removal was performed under ketamine + xylazine anesthesia in the same fashion as mentioned before. All animal procedures were performed in accordance with guidelines set by the National Institutes of Health and the Hungarian law on animal care and protection. The experimental protocol was reviewed and approved by the "Institutional Ethical Committee for Animal Care and Use" of Semmelweis University (registration number: XIV-I-001/2102-4/2012 and XIV-I-001/2104-4/2012).

4.2. Animals and experimental design

We used male rats in all experiments. Sprague-Dawley (SD) rats (Toxicological Research Center (Toxi-Coop, Dunakeszi, Hungary) weighing 230 +/- 10 grams, 12 weeks old obese (fa/fa) and lean (fa/+) Zucker rats (Crl:ZUC-Leprfa, Charles River Laboratories, Sulzfeld, Germany) were used in the diabetic nephropathy study. In the toxic nephropathy study, BH rats were compared to Charles Dawley (CD) rats (both strains from Charles River Ltd. Isaszeg, Hungary) at eight weeks of age. After arrival the animals were allowed 1 week for acclimatization. All animals were maintained under standardized (light on 08:00–20:00 h; 40–70% relative humidity, 22±1°C), specified pathogen-free (SPF) conditions, with free access to water and standard rodent chow (Altromin standard diet, Germany).

4.3. The diabetic nephropathy study

4.3.1. Induction of diabetes

Male SD rats were injected intraperitoneally with 60 mg/kg streptozotocin (Sigma-Aldrich, St. Louis, MO, USA) dissolved in citrate buffer, pH 4.5, in order to induce diabetes. The control group received citrate buffer only (n=5/group). Development of diabetes was confirmed one week after streptozotocin injection by measuring post-prandial blood glucose with Glucostix using Reflotron Plus Automat (Roche, Budaörs, Hungary). Oral glucose tolerance test was performed at sacrifice, four weeks after STZ injection. Urinary albumin excretion was measured before and 4 weeks after STZ injection when the experiment was terminated.

In order to analyze the ezrin expression level in a different animal model of DN 12 weeks old obese (fa/fa) and lean (fa/+) Zucker rats were used. The obese Zucker rats develop severe hyperphagia, obesity and type II. DM-like characteristics spontaneously over time (97).

4.3.2. Urinary albumin determination

Urine was collected for 24 hours in diuresis cages (Techniplas, Italy) before STZ injection for self-control purposes and 4 weeks later, before terminating the experiment.

Urinary albumin was measured in the diabetic nephropathy study by a rat albumin-specific ELISA kit (Immunology Consultants Laboratory Inc, Portland, OR, USA) as described by the manufacturer. Briefly, the 96 well plates (Nunc™ GmbH & Co. KG, Langenselbold, Germany) were coated with diluted capture antibody and the non-specific binding sites were blocked with assay diluent (50 mM Tris, 0.14 M NaCl, 1% BSA, pH 80). Adequately diluted samples were incubated in duplicates for 2 hours on the plate and then the detection antibody was added. Next, Streptavidin-HRP was linked to the detection antibody, followed by a short incubation with TMB Substrate (Sigma-Aldrich GmbH, Germany). A washing session (5 times with 300 µl of washing buffer) was performed between all steps until the addition of the substrate solution. The enzymatic reaction was terminated by stop solution containing H_2SO_4. Optical density was measured with a plate reader (PerkinElmer, Victor3™ 1420 Multilabel Counter, WALLAC Oy, Finland) at 450 nm with wavelength correction set to 544 nm.

Concentrations were calculated with WorkOut (Dazdaq Ltd., England), using a four parameter logistic curve-fit.

4.3.3. Sacrifice and sample collection

The STZ- or citrate-injected SD rats were anesthetized with ketamine + xylazine. To prevent blood clotting, 1 ml/kg Na-Heparin (Sigma-Aldrich Corporation, Saint Louis, MO, USA) was injected intraperitoneally. Rats were bled from the aorto-iliac bifurcation. Animals were perfused through the aorta with 60 ml cold physiological saline to remove blood from the vasculature. After perfusion, both kidneys were removed for further analysis.

One kidney from each animal was used for isolation of glomeruli by graded sieving (98). Briefly, the kidneys are washed in cold (≈4 ^{o}C) phosphate-buffered saline (PBS). The renal capsule was removed, and the cortex was cut into 1 mm^3 pieces. The kidney pieces were gently pressed with a blunt tool through the first metal sieve (150 μm pore size). The leftover tissue was washed three times with cold PBS until most of the glomeruli were collected on the second sieve (pore size: 100 μm). The glomeruli on the second sieve were washed again three times to remove any contamination or unwanted renal tissue fragments such as tubular or interstitial cells. Finally the glomerular fraction was collected from the second sieve into a 15 ml tube in 10-12 ml cold PBS. The collected sample was centrifuged at 1 000 RCF (relative centrifugal force) for 5 minutes. After the supernatant was removed; the isolated glomeruli were stored in approximately 1 ml PBS on -80 ^{o}C (Figure 4).

Isolated glomeruli were used for two-dimensional fluorescence difference gel electrophoresis (2D-DIGE), immunoblotting and indirect immunofluorescence.

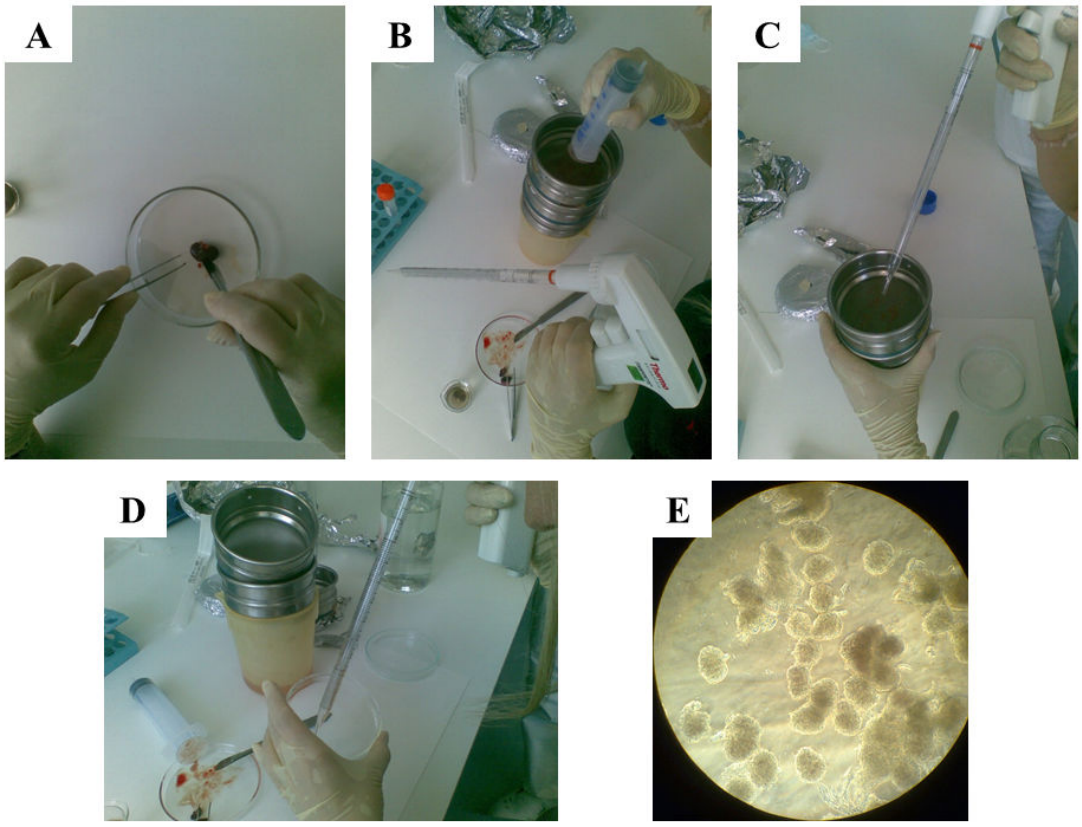

Figure 4: Isolation of glomeruli:

A: Removing the renal capsule

B: Pressing the kidney pieces through the first sieve

C: Washing the leftover kidney tissue

D: Collecting the glomerular fraction

E: Inverted microscopic appearance of the isolated glomeruli (magnification: 40x)

4.3.4. Renal morphology

Ultrastructural changes in glomeruli were visualized by electron microscopy. Kidney samples from the STZ-, and citrate-injected SD rats were fixed in 1.5% glutaraldehyde, 3% paraformaldehyde, 5% sucrose in 0.1 mol/L cacodylate buffer, pH 7.4, at room temperature for 2 hours, followed by postfixation in 1% osmium tetroxide (OsO4) in the same buffer for 1 hour. Samples were stained en bloc in 1% uranyl acetate in 10% ethanol for 1 hour, dehydrated in ethanol and embedded in Epon. Thin sections were stained with uranyl acetate and lead citrate and examined in a JEM-1400 Transmission Electron Microscope (Jeol) equipped with transmission electron microscopy charge-coupled device (TEM CCD) camera (Olympus Soft Imaging Solutions GmbH, Japan).

4.3.5. Two-dimensional fluorescence difference gel electrophoresis

The isolated glomeruli from the diabetic or the control SD rats were lysed in 7 mol/L urea, 2 mol/L thiourea, 4% 3-[(3-cholamidopropyl)-dimethylammonio]-1-propanesulfonate (CHAPS), 30 mmol/L Tris-HCl, pH 8.0, 0.2% sodium dodecyl sulfate (SDS), sonicated for 3x15 sec and centrifuged at 13,000 RCF for 15 min. Protein concentrations were measured with 2D Quant Kit (GE Healthcare, Chalfont St. Giles, UK). 50 μg glomerular lysate from rats with STZ-induced diabetes or controls were labeled individually with Cy3 and Cy5, respectively, using CyDye DIGE Fluor minimal labeling kit (GE Healthcare), following manufacturer's instructions. An internal standard (a pool of all samples) was labeled with Cy2. Isoelectric focusing was performed using linear pH 3-10, 24 cm Immobiline™ DryStrips (GE Healthcare). The strips were equilibrated in 6 mol/L urea, 2% SDS, 1% dithiothreitol (DTT), 30% glycerol, and 75 mmol/L Tris-HCl, pH 8.8, followed by incubation in the same solution, but replacing DTT with 2.5% iodoacetamide. Proteins were resolved in 12% polyacrylamide gels at 10 W/gel for 16 hours and imaged with Typhoon 9400 (GE Healthcare). A comparison of the images was performed using DeCyder 2D 7.0 software (GE Healthcare). Reference gel was randomly selected from the control gels, and spots from the other gels were matched to those in the reference gel. The intensities of the spots were normalized by dividing each Cy3 or Cy5 spot volume with the corresponding Cy2 (internal standard) spot volume. Normalized intensities of matched spots were compared between the groups, and spots with intensity changes >1.5-fold with a confidence interval (CI) above 95% (student's *t*-test ANOVA analyses; $p < 0.05$) was considered differentially expressed and significant.

4.3.6. Identification of proteins by LC-MS/MS

Spots of interest were excised from a silver-stained 2D SDS-PAGE gel, in-gel digested with trypsin, and the resulting peptides were analyzed by liquid chromatography tandem mass spectrometry (LC-MS/MS) using an Ultimate 3000 nano-LC (Dionex, Sunnyvale, CA, USA) and a QSTAR Elite hybrid quadrupole time-of-flight MS (Applied Biosystems/MDS Sciex, Life Technologies, Carlsbad, CA, USA) with nanoelectrospray ionization, as described previously (99). The LC-MS/MS data were searched with in-house Mascot through ProteinPilot 2.0 interface against the SwissProt database using

the following criteria: rodent-specific taxonomy, trypsin digestion with one missed cleavage allowed, carbamidomethyl modification of cysteine as a fixed modification, and oxidation of methionine as a variable modification. All of the reported protein identifications were statistically significant ($P < 0.05$).

4.3.7. Immunoblotting

Glomerular lysates of three individual STZ-injected and three individual control rats were used for confirming the 2D-DIGE results. Glomerular lysates of 12 weeks old six individual obese (fa/fa) and six individual lean (fa/+) Zucker rats were used for analyzing the expression level of ezrin in type 2 diabetes. Immunoblotting was performed as previously described (100,101). Briefly, 20 μg protein were separated by 10% sodium dodecyl sulfate-polyacrylamide gel electrophoresis (SDS-PAGE) and transferred to polyvinylidene difluoride membranes (Millipore, Billerica, MA, USA). After blocking with 5% nonfat milk in Tris-buffered saline supplemented with 0.1% Tween-20 (TBS-Tween) for 1h at room temperature, membranes were incubated with primary antibodies diluted in 1% nonfat milk in TBS-Tween at room temperature (1 hour) followed by secondary antibodies conjugated with IRDye 680 or 800 (LI-COR, Lincoln, NE, USA). Blots were scanned and quantified using an Odyssey Infrared Imaging System (LI-COR).

4.3.8. Immunohistochemistry of rat kidney samples

Rat kidney cryosections from the STZ-, or citrate-injected SD rats were fixed with acetone, blocked with CAS-BLOCK (Invitrogen) and stained with mouse anti-ezrin, rabbit anti-phospho-ezrin, rabbit anti-NHERF2 and rabbit anti-podocin diluted in ChemMate (DakoCytomation) at 4°C overnight (102). Detection was with AlexaFluor 555 donkey anti-rabbit and AlexaFluor 488 donkey anti-mouse IgGs (Molecular Probes). Samples were examined with Zeiss Axioplan2 microscope (Carl Zeiss Microscopy GmbH, Jena, Germany) or Leica TCS SP8 MP CARS confocal microscope (Leica Microsystems, Wetzlar, Germany).

4.3.9. Immunohistochemistry of human kidney samples

Kidney samples of renal cancer patients with or without type 2 diabetes were obtained from surgical nephrectomies performed for diagnostic purposes at Helsinki and Uusimaa Hospital district, and were from the nonmalignant part of the kidney. Albuminuria, the clinical sign of diabetic nephropathy, was determined from the medical records. Kidney samples were fixed with 10% formalin, dehydrated, and embedded in paraffin and stained for ezrin. Briefly, after the sections were deparaffinized, antigen retrieval was performed by boiling for 15 min in a microwave oven in 10 mM citric acid, pH 6.0 and endogenous peroxidase was inactivated by incubation in hydrogen peroxide in methanol for 30 min. Sections were blocked with CAS-block (Invitrogen, Carlsbad, CA, USA) and incubated with anti-ezrin primary antibodies diluted in ChemMate™ (DakoCytomation, Glostrup, Denmark) overnight at 4C. Sections were washed in phosphate-buffered saline (PBS) and incubated with biotinylated secondary antibodies for 30 min, followed by incubation with ABC-reagent and AEC (Sigma-Aldrich, St. Louis, MO, USA) for color development. Sections were counterstained with hematoxylin, mounted with Shandon Immu-Mount (Thermo Scientific, Waltham, MA, USA) and examined by light microscope. Glomeruli (six/sample) were analyzed from 13 patients with type 2 diabetes and 14 controls. The staining intensity of ezrin was visually graded by two researchers independently and blinded from the diabetes status. For histopathological analysis the kidney samples were stained with PAS. The use of human material was approved by the local Ethics Committee.

4.4. The toxic nephropathy study

4.4.1. Induction of toxic glomerular damage

In the toxic nephropathy experimental series we performed the following two experiments:

1. Renal functional and morphological experiment in DXR-induced renal failure;
2. Long term survival study;

In the functional and morphological experiment (exp. 1) rats from both strains (n = 8/group) were intravenously injected with 5 mg/kg body weight DXR (Sicor S.r.l. Società Italiana Corticosteroidi, Italy) dissolved in saline. The BH and CD rats in the

negative control groups were injected with equal volume of saline only. DXR dose was based on literature data and pilot experiments: 2 mg/kg DXR did not induce renal damage, whereas 8 mg/kg DXR caused premature moribund state in some animals. Urinary protein and NGAL excretion was followed for 8 weeks when the experiment was terminated and renal morphology was investigated. Survival (exp. 2) was evaluated in age matched BH and CD rats (n = 8/group) (5 mg/kg DXR, iv). In the survival experiment animals were euthanized upon signs of uremia. Blood urea was > 250 mg/dl in each euthanized animal demonstrating that uremia was the cause of the moribund state.

In order to investigate whether the difference in the degree of tubulointerstitial fibrosis between the two rat strains was the consequence of different tubular protein load, or BH rats were resistant to tubulointerstitial fibrosis per se, we formed two sub-groups. In this analysis CD and BH rats injected with DXR (CD/DXRp, n = 4 and BH/DXRp, n = 5) were matched for urinary protein excretion and sensitive tubular, inflammatory and fibrosis parameters were compared.

4.4.2. Urinary protein and NGAL determinations

In the renal functional and morphological experiment urine was collected for 24 hours in diuresis cages before and biweekly after DXR injection until the 8th week , when the experiment was terminated. 24 hours total urine protein excretion was measured with a pyrogallol red colorimetric assay (Diagnosticum Ltd, Budapest, Hungary). Briefly, the assay was carried out on 96 well plates (Greiner Bio-One GmbH, Germany). Four µl sample and 200 µl Reagent 1 (provided by the assay, Cat.No: 425051/DC) were added, mixed and incubated for 10 minutes on 37°C. Optical density was measured at 598 nm with the SpectraMax 340 Microplate Spectrophotometer (Molecular Devices, Sunnyvale, USA). Concentrations were calculated with SoftMax® Pro Software.

Urine NGAL levels were measured with rat Lipocalin-2/NGAL DuoSet ELISA Development kit (R&D Systems, USA) according to the manufacturer's instructions, in a similar fashion as the determination of urinary albumin.

4.4.3. Sacrifice and sample collection

When the experiments were terminated the rats were anesthetized with ketamine + xylazine. To prevent blood clotting, 1 ml/kg Na-EDTA (Sigma-Aldrich Corporation, Saint Louis, MO, USA) was injected intraperitoneally. Rats were bled from the aorto-iliac bifurcation. Like in the diabetic nephropathy study, animals were perfused through the aorta with 60 ml cold physiological saline to remove blood from the vasculature. Both kidneys and the heart were removed. The heart and a third of the left kidney were fixed in 4% buffered formaldehyde and were later embedded in paraffin for basic histological and immunohistochemical analysis. The remaining two thirds of the left kidney cortex and medulla were separated, frozen in liquid nitrogen and stored at -80°C for molecular studies.

4.4.4. Renal morphology

Kidney paraffin sections form the DXR-, or saline-injected rats were stained with hematoxylin-eosin (HE), periodic acid–Schiff (PAS), or Picro-Sirius Red. Glomerulosclerosis was assessed on PAS stained sections according to a modified (96,103) scoring system (scores 0–4) of El Nahas et al. (104) at x400 absolute magnification using an Olympus CX21 microscope (Olympus Optical Co. Ltd., Japan). Score 0: normal glomerulus. Score 1: thickening of the basement membrane. 2: mild (<25%), 2.5: severe segmental (>50%) and 3: diffuse hyalinosis. 4: total tuft obliteration and collapse. The glomerular score of each animal was derived as the arithmetic mean of 100 glomeruli.

Tubulointerstitial damage was assessed with a semiquantitative scale (magnification ×100) of percent area affected by tubulointerstitial changes (90,105). Score 0: normal tubules and interstitium, 1: brush border loss or tubular dilatation in <25% of the field of view (fv). 2: tubular atrophy, dilation and casts in < 50% fv. Score 3: tubular and interstitial damage in < 75% fv, 4: tubular atrophy, dilation, casts and fibrosis > 75% fv. The overall score was the mean of 15 fvs.

Inflammatory infiltration was assessed on hematoxylin-eosin stained sections as the percent of area infiltrated by inflammatory cells (magnification: x400). Score 0: normal glomeruli, tubules and interstitium, 1: inflammatory cells present in <25% fv. 2:

inflammation in < 50% fv. Score 3: inflammation in < 75% fv, 4: inflammation in > 75% of fv. The overall score was the mean of 120 fvs.

Collagen deposition in the renal interstitium was demonstrated by Picro-Sirius Red staining as described previously (106,107) . Fibrotic areas were quantified using Image J software (National Institutes of Health, Bethesda, Maryland, US).

4.4.5. Immunoblotting

Renal cortex samples from the DXR-, or saline-injected CD and BH rats were lysed in RIPA Buffer (Thermo Scientific, Rockford, IL). Protein concentration was determined by the bicinchoninic acid (BCA) protein assay (Thermo Scientific, Rockford, IL).

Twenty μg protein was resolved on 4–12% Criterion XT Bis-Tris Precast gels (BioRad, Hercules, CA) and transferred to nitrocellulose membrane to detect 4-hydroxy-2-nonenal (HNE) or to Polyvinylidene Difluoride (PVDF) membrane to detect nitrotyrosine (NT). The primary NT antibody was applied at 1.3 μg/mL and the primary HNE antibody at 0.3 μg/mL. The secondary antibody (peroxidase conjugated goat anti-mouse, PerkinElmer, Santa Clara, CA) was applied at 0.25 μg/mL. Blots were incubated in enhanced chemiluminescence substrate, Supersignal West Pico Chemiluminescent Substrate (Thermo Scientific, Rockford, IL), and were exposed to photographic film. After stripping membrane with Restore Western Blot Stripping Buffer (Thermo Scientific, Rockford, IL), as a loading control, peroxidase conjugated anti-actin (AC-15 Abcam, Cambridge, MA) was applied at 70 ng/mL concentration in blocking buffer for 1 h at room temperature.

4.4.6. Immunohistochemistry of rat kidney samples

Rat kidney paraffin sections on Superfrost Ultra Plus Adhesion Slides (Thermo Fisher Scientific Inc, Waltham, MA, USA) from the DXR-, or saline-injected BH and rats were deparaffinized and rehydrated in ethanol. Fibronectin immunohistochemistry was performed with anti-fibronectin antibody (1:2000), using the avidin–biotin method (108). Antigen retrieval was performed in citrate buffer (pH: 6.0) for 20 min in a microwave oven at 750W power. Samples were cooled on bench for 20 min, washed in dH2O then washed in 0.1 M Tris-buffered saline pH 7.4 (TBS) for 5 minutes. Blocking of non-specific protein binding was performed using 2% goat serum in TBS. The

sections were incubated with the primary antibodies overnight at 4C. Samples were washed in TBS and incubated with goat anti-rabbit secondary antibody (Rabbit Link, Biogenex, USA) for 20 min, washed and incubated with alkaline phosphatase-conjugated streptavidin (AP Link, Biogenex) for another 20 min. Slides were developed after washing in TBS with FastRed (Dako, USA) for 10 min. The sections were counterstained with hematoxylin and mounted with Aquatex (Merck, Germany). Pictures were taken from the stained sections for further analysis. The fibronectin stained area was quantified with Image J software.

HNE and NT immunohistochemistry was performed in a similar fashion as described previously, with mouse monoclonal antibody (HNE clone: HNEJ-2, JaICA, Japan; NT clone: #189542, Cayman Chemical Company, Michigan, IL). Color development was induced by incubation with diaminobenzidine (DAB) kit (Vector Laboratories, Burlingame, CA).

4.4.7. Heart fibrosis markers

In a separate group of DXR-injected BH and CD rats, the hearts were removed and fixed in 4% buffered formalin and embedded similarly to the renal samples 8 weeks after 5 mg/kg DXR administration. Consecutive sections were stained with Masson's trichrome to detect collagen deposition as a sign of chronic fibrosis, and direct immunofluorescence was performed for connexin-43 (Cx43, 1:100), an early marker of cardiomyocyte damage. Briefly, paraffin sections were dewaxed in xylole, and then gradually rehydrated in ethanol, then washed in dH_2O. Antigen retrieval was performed in Tris-EDTA buffer (pH: 9.0) for 50 min in a microwave oven at 750W power. Samples were cooled on bench for 20 min, washed in dH2O then washed in 0.1 M Tris-buffered saline pH 7.4 (TBS) for 5 minutes. Blocking of non-specific protein binding was performed using 1 % BSA. The sections were incubated with the rabbit anti-Cx43 and mouse anti-desmin primary antibodies overnight at 4C. Samples were washed in TBS and incubated with either Alexa488 (green) or Alexa546 (orange-red) labeled anti-mouse or anti-rabbit IgG, diluted in 1 : 200 (all from Invitrogen-Molecular Probes, Carlsbad, CA) for 90 min without exposure to light. After washing in TBS, sections were counterstained with Hoescht (blue). Finally the slides were mounted with a gelatin-based medium Faramount (Santa Clara, California, USA).

4.4.8. Monitoring mRNA levels with Real-Time quantitative Polymerase Chain Reaction (RT-qPCR)

Total RNA for RT-qPCR was extracted by homogenizing 50-80 mg pieces of renal cortex in TRI Reagent (Molecular Research Center Inc., Cat. No.: TR118) according to the manufacturer's protocol. Briefly, RNA was precipitated by chloroform and isopropyl alcohol. The RNA pellet was washed twice with 75% ethanol, resolved in RNase free water (Lonza Group Ltd, Basel, Switzerland) and stored at -80 ^{o}C. DNA contamination was removed by TURBO DNase (Life technologies, Ambion, Cat. No: AM2238). DNase activity was terminated by adding 50 µl phenol-chloroform-isoamylalcohol to 50 µl of DNase-digested RNA solution. RNA concentration and purity was measured with the NanoDrop 2000c Spectrophotometer (Thermo Fisher, USA). The RNA integrity was verified by electrophoretic separation on 1% agarose gel. Reverse transcription of 1 µg total renal RNA into cDNA was carried out using random hexamer primers and the High-Capacity cDNA Archive Kit (Applied Biosystem, USA) according to the manufacturer's protocol. Messenger RNA levels of NADPH oxidase-2 (NOX-2, p91^{phox}, cytochrome b-245 beta polypeptide), neutrophil cytosolic factor 1 (Ncf1, p47^{phox}), collagen type I, alpha 1 (COL1A1), transforming growth factor β1 (TGF-β1), connective tissue growth factor (CTGF) and macrophage chemotactic protein 1, (MCP-1, chemokine (C-C motif) ligand 2, Ccl2) were measured by RT-qPCR (Qiagen, Hilden, Germany) and target mRNA levels were normalized to actin mRNA levels (Table 1).

Table 1: Qiagen primer reference numbers.

Gene	**Reference sequence**	**Qiagen primer reference number**
p91^{phox} (NOX2)	NM_023965.1	QT00195300
p47^{phox} (Ncf1)	NM_053734	QT00189728
MCP-1 (Ccl2)	NM_031530.1	QT00183253
TGF-β1	NM_021578.2	QT00187796
CTGF	NM_022266.2	QT00182021
COL1A1	NM_053304.1	QT02285619

Nephrin mRNA levels were measured by double-stranded DNA (dsDNA) dye based RT-qPCR with Maxima SYBR Green RT-qPCR Master Mix (Thermo Fisher Scientific Inc., Waltham, MA, USA), and the mRNA values were normalized to glyceraldehyde-3-phosphate dehydrogenase. Mean values are expressed as fold mRNA levels relative to the control using the formula $2^{-\Delta(\Delta Ct)}$ (CT: cycle time, $\Delta CT = CT_{target} - CT_{normalizer}$ and $\Delta(\Delta CT) = \Delta CT_{stimulated} - \Delta CT_{control}$) (109).

4.5. Antibodies

Antibodies used in the diabetic nephropathy study were mouse anti-ezrin (clone 3C12) (110), rabbit anti-phospho-ezrin (Santa Cruz Biotechnology, Santa Cruz, CA, USA), rabbit anti-NHERF2 (kindly provided by Dr. Peijian He, Emory University, Atlanta, GA, USA), mouse anti-podocalyxin, rabbit anti-podocin and mouse anti-α-tubulin (Sigma-Aldrich, St. Louis, Missouri, USA).

Antibodies used in the toxic nephropathy study were mouse monoclonal anti-4-hydroxy-2-nonenal (HNE, clone: HNEJ-2, JaICA, Japan), mouse monoclonal anti-nitrotyrosine (NT, #189542, Cayman Chemical Company, Michigan, IL) rabbit polyclonal anti-fibronectin (Sigma-Aldrich, St. Louis, Missouri, USA), rabbit anti-Cx43 (, #3512, Cell Signaling, Beverly, MA, USA) and mouse anti-desmin (Agilent Technologies, Santa Clara, California, USA).

4.6. Statistics

Unpaired t-test was used to evaluate the differences between the STZ-injected and the citrate-injected control SD rats, also to compare the variables of the two sub-groups within the BH/DXR and the CD/DXR groups. χ^2 test was used to examine the sex distribution of the patients, whose kidney samples were analyzed. Two-way ANOVA with or without repeated measures was used for multiple comparisons. Post hoc analyses were done with Holm-Sidak‘s test. Logarithmic transformation of data was used if Bartlett’s test indicated a significant inhomogeneity of variances. Survival was analyzed according to the Kaplan-Meier method. The null hypothesis was rejected if $p < 0.05$. Data are expressed as means ±SD. Statistical analysis was done with GraphPad Prism (version 6.01, GraphPad Software Inc, San Diego, CA, USA).

DOI:10.14753/SE.2018.1981

5. Results

5.1. Results of the diabetic nephropathy study

5.1.1. Streptozotocin-induced diabetes led to differential expression of glomerular proteins

To characterize the early molecular changes associated with the development of diabetic kidney injury, we compared total soluble protein fractions of glomeruli isolated from rats with streptozotocin-induced diabetes and controls using 2D-DIGE coupled with mass spectrometry. To identify changes at an early stage of disease, we performed the analysis 4 weeks after induction of diabetes. The streptozotocin-injected rats used for the analysis were albuminuric and had high blood glucose compared with controls (Figure 5, A and B), but did not show ultrastructural changes in the glomeruli (Figure 6, A and B). Lysates prepared from glomeruli isolated from five individual streptozotocin- and five citrate buffer-injected rats were labeled with Cy3 and Cy5, respectively, and an internal control (a pool of all glomerular samples prepared from diabetic and control rats) used for normalization was labeled with Cy2. Analysis with DeCyder software revealed 2274 spots that were present in all five gels. Of the 2274 spots, 29 exhibited a statistically significant (Student's t-test value ≤ 0.05) difference >1.5-fold between the diabetic and control rat glomerular samples. Fifteen spots were up-regulated (maximum, 3.16-fold) and 14 were down-regulated (maximum, 3.11-fold) in the diabetic kidney glomeruli. Of the 29 differentially expressed spots, mass spectrometry identified multiple proteins in 17 spots, and a single protein in 12 spots, including actin binding and actin cytoskeleton organizing proteins, apoptosis-associated proteins, regulators of oxidative tolerance and DNA binding, and repair proteins.

DOI:10.14753/SE.2018.1981

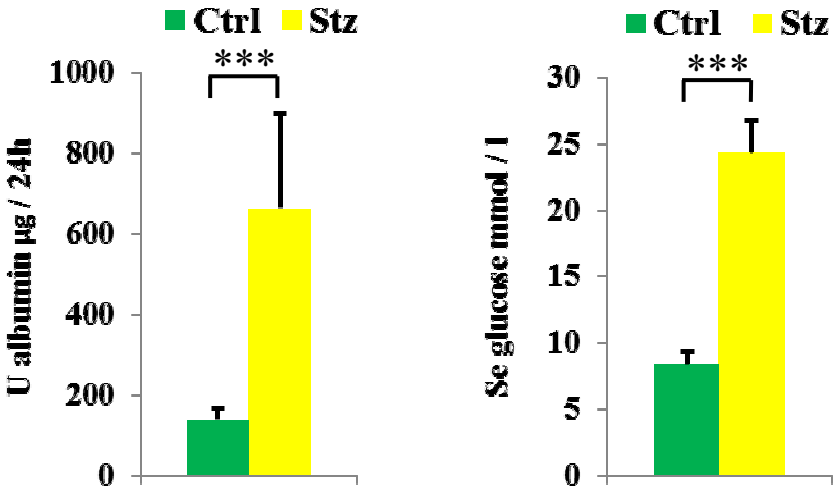

Figure 5: Urinary albumin (A) and blood glucose (B) levels in Streptozotocin-injected and control rats.

Ctrl: citrate buffer-injected SD rats, Stz: Streptozotocin-injected SD rats. n=5/group

***: $p<0.001$ vs. the negative control group of the same strain.

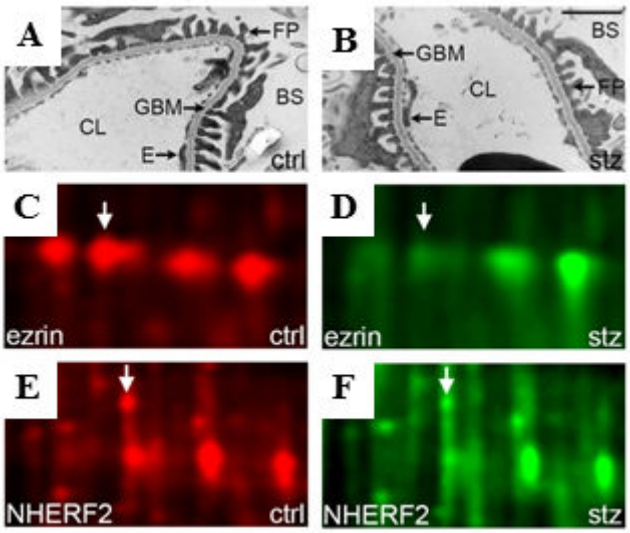

Figure 6: Electron microscopy of control (ctrl; A) and streptozotocin-injected (stz; B) rats. Selected regions of the 2D-DIGE gel showing the spots representing ezrin (arrows, C and D) and NHERF2 (arrows, E and F).

BS: Bowman's space; CL: capillary lumen; E: glomerular endothelial cells; FP: podocyte foot process; GBM: glomerular basement membrane.

Scale bar = 1 µm (A and B).

DOI:10.14753/SE.2018.1981

5.1.2. Ezrin and NHERF2 were down-regulated in the glomeruli of diabetic rats

Although it is well documented that the organization of the actin cytoskeleton in podocytes is altered in several types of glomerular diseases, (34) little is known about the regulatory proteins that control actin dynamics in podocytes in diabetic nephropathy. We, therefore, chose the cytoskeletal linkers ezrin and NHERF2 (40) for further analysis. Ezrin and NHERF2 were both single identifications in the mass spectrometry, and showed 2.1- and 1.94-fold decreases in diabetic glomeruli (Figure 6, C-F). Semiquantitative Western blot analysis confirmed that treatment with streptozotocin decreased the amount of ezrin by 49% and NHERF2 by 42% compared with citrate-injected rat glomeruli (Figure 7, A and B). Phosphorylation of ezrin at threonine 567 was reduced by 49%, indicating that both the total amount and the active ezrin are decreased in the glomeruli of rats with experimental diabetes. Also, podocalyxin, which is connected to actin through ezrin/NHERF2 complex, (98) was down-regulated by 35% in the glomeruli of streptozotocin injected rats, confirming previous findings (111). The expression of podocin remained unchanged (Figure 7, A and B). Immunostaining revealed decreased expression of ezrin, NHERF2, and phosphorylated ezrin (p-ezrin) in the glomeruli of diabetic rats (Figure 8, A-C and E-G), whereas podocin expression remained unchanged (Figure 8, D and H), further confirming the 2D-DIGE and semiquantitative Western blot results.

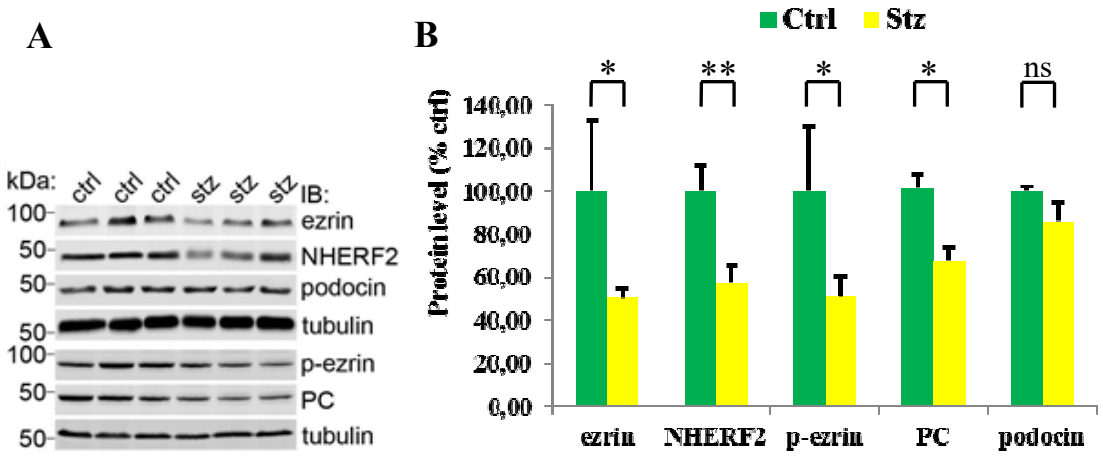

Figure 7: Protein levels in Streptozotocin-injected and control rats.

A: Western blot results, **B**: Quantification of ezrin, NHERF2, p-ezrin, podocalyxin (PC), and podocin levels. Tubulin is included as a loading control.

Ctrl: citrate buffer-injected SD rats, Stz: Streptozotocin-injected SD rats n=5/group

*: $p<0.05$ vs. the negative control group of the same strain.

DOI:10.14753/SE.2018.1981

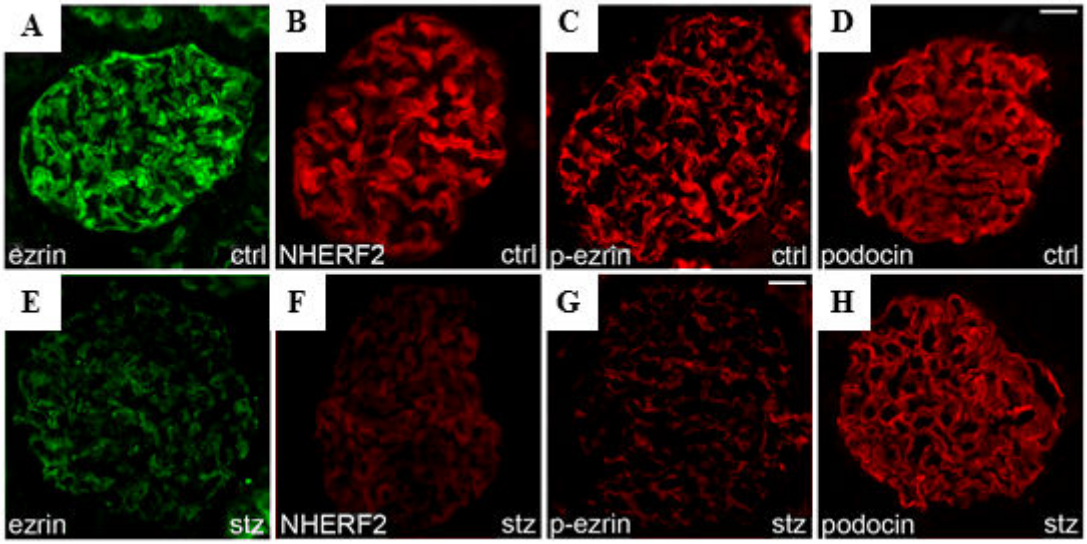

Figure 8: Immunofluorescence images of glomeruli of control (A-D) and streptozotocin-injected (E-H) rats stained for ezrin, NHERF2, phosphorylated ezrin (p-ezrin), and podocin.

Ctrl: saline-injected, stz: Streptozotocin-injected rats. Scale bar = 30 µm.

5.1.3. Expression of ezrin was reduced in glomeruli of obese Zucker rats and in glomeruli of patients with type 2 diabetes

Next, we investigated the expression of ezrin in glomeruli of 12-week-old obese Zucker rats and their age-matched lean controls. Obese Zucker rats are insulin resistant and slightly diabetic because of a mutation in the leptin receptor gene, and they develop albuminuria by 40 weeks of age (112,113). Semiquantitative Western blot analysis revealed that the expression of ezrin was decreased by 20% in glomeruli of obese Zucker rats when compared with that in lean Zucker rats (Figure 9).

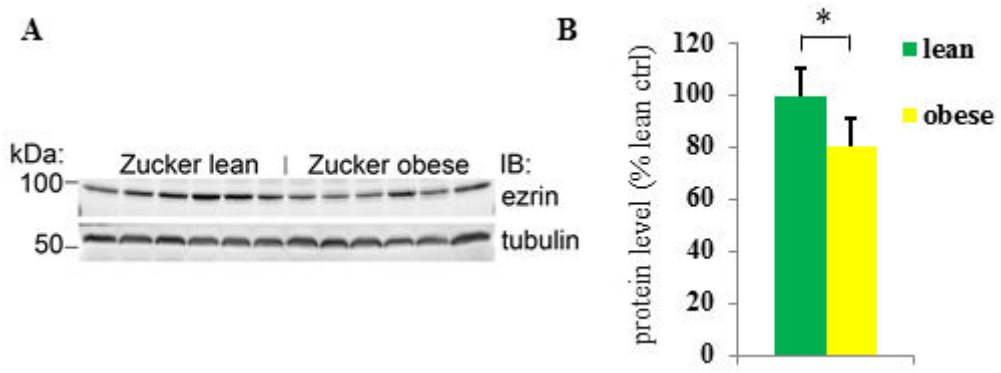

Figure 9: Ezrin protein levels in obese Zucker rats

A: Western blot results. B: Quantification of ezrin levels in (A). n=5/group Tubulin is included as a loading control. *: $p<0.05$ vs. negative control group.

DOI:10.14753/SE.2018.1981

The expression of ezrin was also studied by immunohistochemistry (IHC) in human kidney samples obtained from nephrectomies. The staining intensity of ezrin was visually graded in glomeruli from 13 patients with type 2 diabetes and 14 controls. The patients did not have clinical nephropathy, and histopathological analysis revealed no diagnostic signs of diabetic nephropathy. The mean age was similar in the groups: 69.2 ± 9.6 years for patients with diabetes and 69.5 ± 12.2 years for controls (P = 0.95, Student's t-test). The sex distribution did not differ significantly between the groups: there were 8 men and 5 women in the group of patients with diabetes and 11 men and 3 women in the control group (P = 0.33, χ^2 test). The expression of ezrin was significantly lower in glomeruli of patients with diabetes (Figure 10).

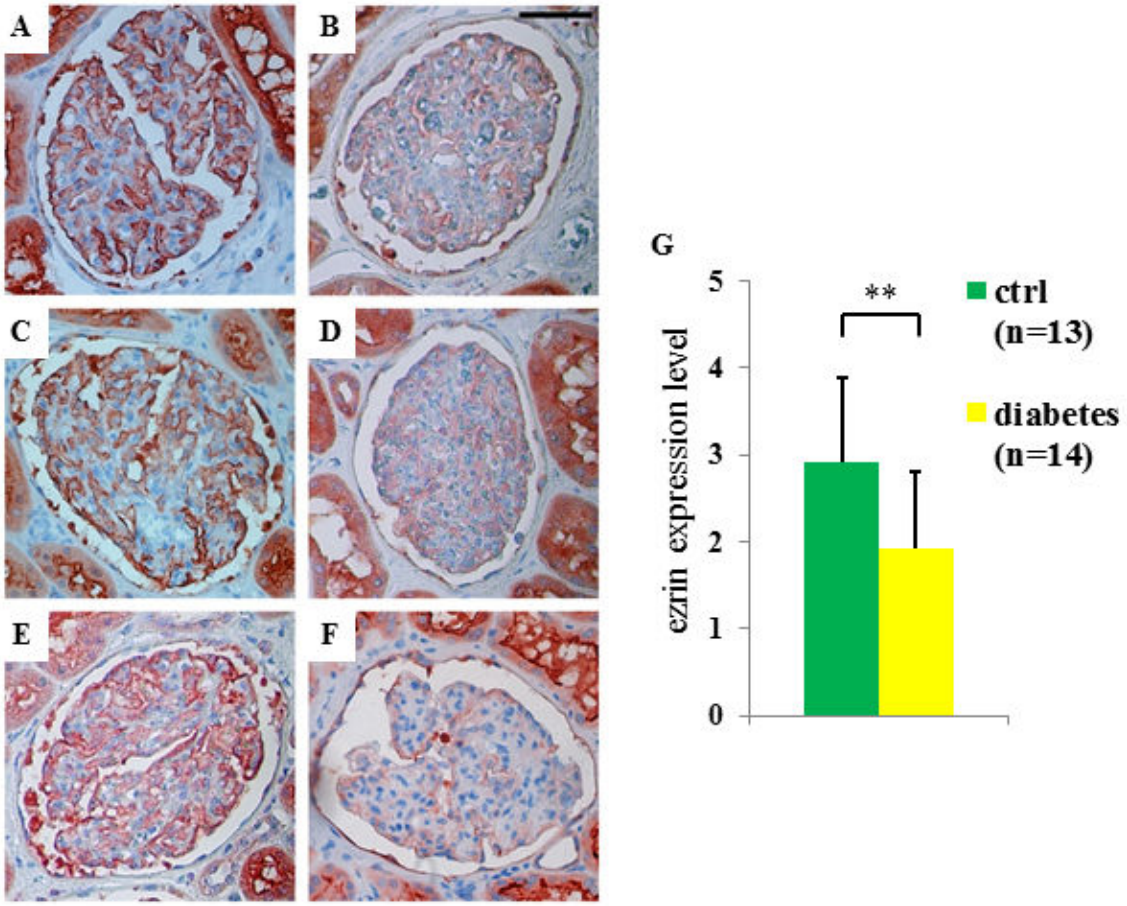

Figure 10: Immunoperoxidase staining for ezrin in glomeruli of controls (A, C, and E) and patients with diabetes (B, D, and F). G: Quantitation of ezrin staining.

Ctrl: control patients.

**: p<0.01 vs. negative control group. Scale bar = 50 µm (B).

DOI:10.14753/SE.2018.1981

5.2. Result of the toxic nephropathy study

5.2.1. Heart toxicity was absent 8 weeks after injection with DXR at 5 mg/kg

Histology of the heart did not show necrosis or other morphological alterations of cardiomyocytes. Massons's trichrom staining was devoid of collagen deposition, and connexin-43 immunostaining did not demonstrate any sign of cardiomyocyte damage. Thus, a single dose of 5 mg/kg DXR did not induce any detectable chronic heart damage (Figure 11).

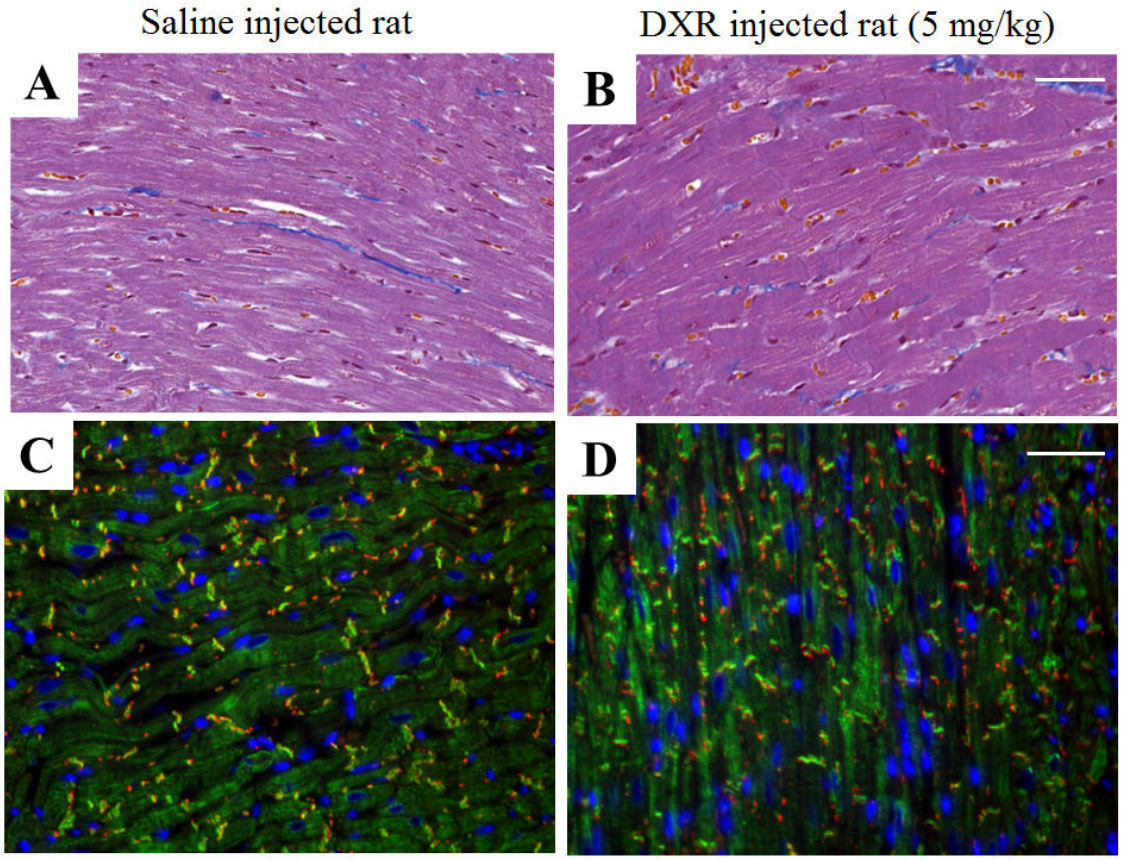

Figure 11: Myocardial morphology and immunohistochemistry:

A, B: Masson's Trichrome staining; C,D: desmin-connexin-43 (CXN-43) immunofluorescent staining (red: CXN-43, green: desmin, blue: nucleus). A and C: saline-injected rat, B and D: doxorubicin-injected rat (dose: 5 mg/kg).

Scale bar = 50 µm (B,D).

5.2.2. CD rats became moribund earlier than BH rats

BH rats became moribund significantly later following the 5 mg/kg DXR dose, compared to CD rats (Figure 12). The first CD rat became moribund 75 days after DXR administration, and there were no survivors after day 90 from this strain. The first BH became moribund 86 days after DXR, and there were survivors even 159 days after DXR administration. The mean survival after DXR was 85 days for the CD rats, while it was 108 days for the BH rats ($p<0.05$). DXR administration caused less severe kidney damage than subtotal nephrectomy (SNX) and salt + protein loading in our previous study (96) as demonstrated by longer survival.

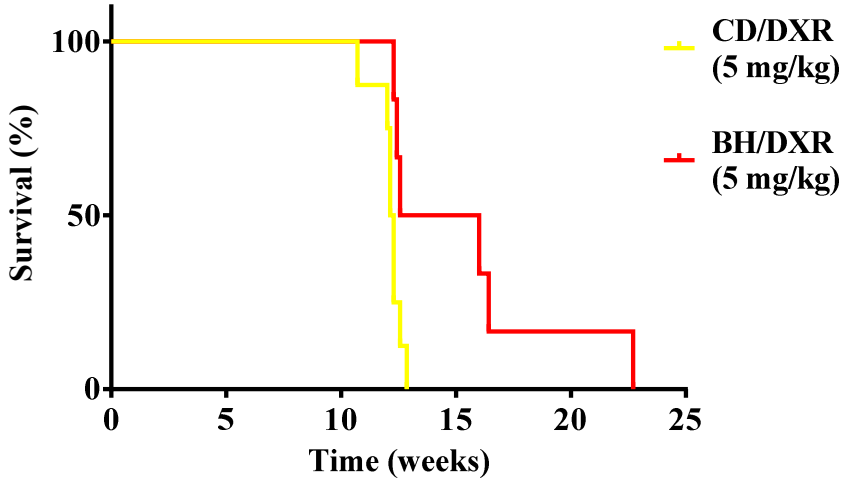

Figure 12: Survival of the Doxorubicin-injected rats.

CD/DXR: Doxorubicin-injected Charles Dawley rats (n=8/group), BH: Doxorubicin-injected Rowett, black hooded rats (n=6/group).

5.2.3. DXR inhibited bodyweight gain more in CD than in BH rats

DXR-administration inhibited weight gain both in BH and CD rats (72). BH rats had a slower growth rate than age matched CD rats. Bodyweight constantly increased in all control animals. Compared to strain identical controls, body weight gain was significantly inhibited in DXR-injected CD rats (CD/DXR) already starting at week 4 On the contrary, significant weight gain reduction was observed in BH rats (BH/DXR) only at week 8 (Figure 13).

DOI:10.14753/SE.2018.1981

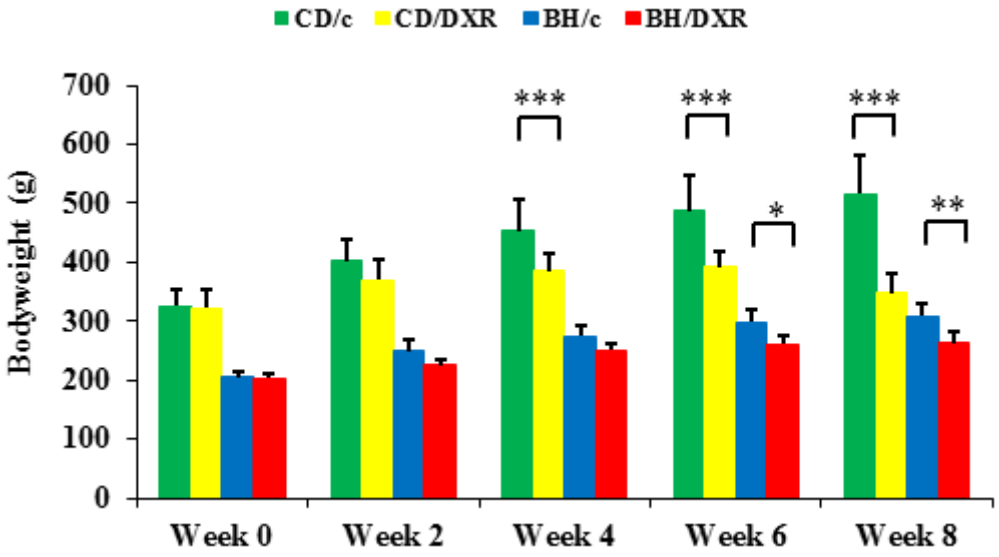

Figure 13: Body weight changes

CD: Charles Dawley rats, BH: Rowett, black hooded rats, /c: Saline-injected control rats, /DXR: doxorubicin-injected rats. (dose: 5 mg/kg). n=8/group

*: $p<0.05$ vs. the negative control group of the same strain, †: $p<0.05$ vs. CD/DXR, positive control group.

5.2.4. Proteinuria was milder in BH than in CD rats after DXR-injection

Proteinuria was assessed as a marker of glomerular damage in the functional and morphological experiment (exp. 1). Treatment with 5 mg/kg DXR induced progressive proteinuria commencing 2 weeks after the DXR injection in CD rats (Figure 14, A). Proteinuria started later and progressed slower, and proteinuria was significantly milder at each time point in BH/DXR rats.

Urinary NGAL —a marker of distal tubular epithelial damage-increased in both DXR-injected groups after 4 weeks. Similarly to proteinuria, NGAL excretion was significantly milder in the BH/DXR group at all times (Figure 14, B).

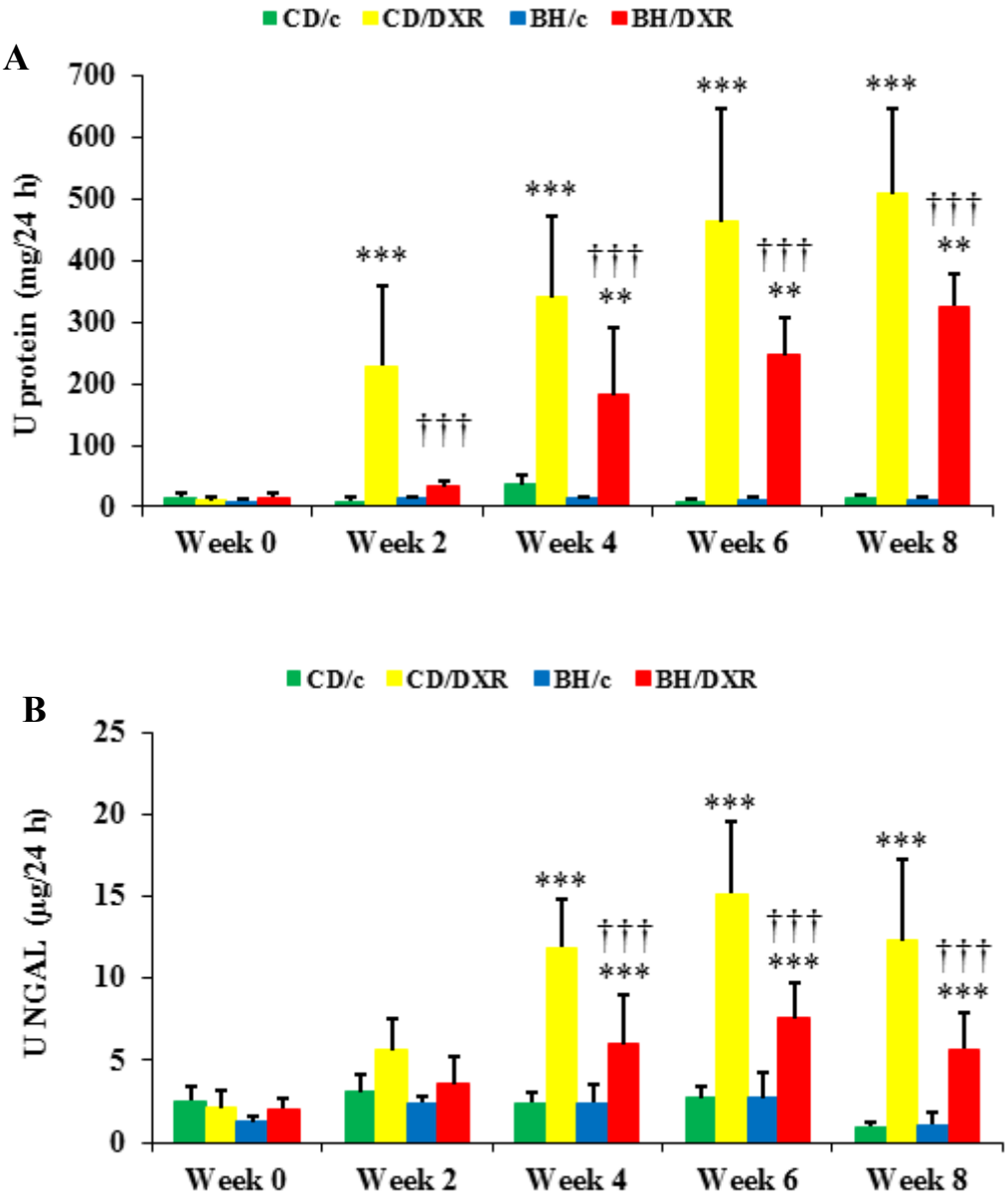

Figure 14: Proteinuria (A) and urinary NGAL excretion (B) in Doxorubicin-injected and control rats.

CD: Charles Dawley rats, BH: Rowett, black hooded rats, /c: Saline-injected control rats, /DXR: doxorubicin-injected rats. (dose: 5 mg/kg). n=8/group

*: $p<0.05$ vs. the negative control group of the same strain, †: $p<0.05$ vs. CD/DXR, positive control group.

5.2.5. Renal histological damage and inflammation were more severe in CD than in BH rats

Both CD and BH rats injected with saline had normal kidney morphology with no or minimal glomerular and tubular abnormalities 8 weeks after the injection. The DXR-

injected BH and CD rats developed FSGS-like lesions, a portion of the nephrons were affected (114). In parallel with milder proteinuria, BH/DXR rats had significantly more intact glomeruli (Score: 0). Mildly (Score: 0.5–1.5) (CD: 50.7 vs. BH: 28.4%) and severely (Score ≤ 2) (CD: 13.3 vs. BH: 3.3%) damaged glomeruli were significantly more common in CD/DXR rats (Figure 15, A–C; Table 2). Probably as a consequence of different degrees of glomerular damage, tubulointerstitial damage was milder in BH rats compared to CD rats (Figure 15, D-F; Table 2). Eight weeks after DXR administration severe inflammatory infiltration by neutrophil granulocytes, lymphocytes and macrophages was evident in the kidney samples of DXR-injected CD rats. In parallel with less proteinuria and morphological damage, inflammation was significantly milder in BH/DXR rats. (Figure 15, G–I; Table 2).

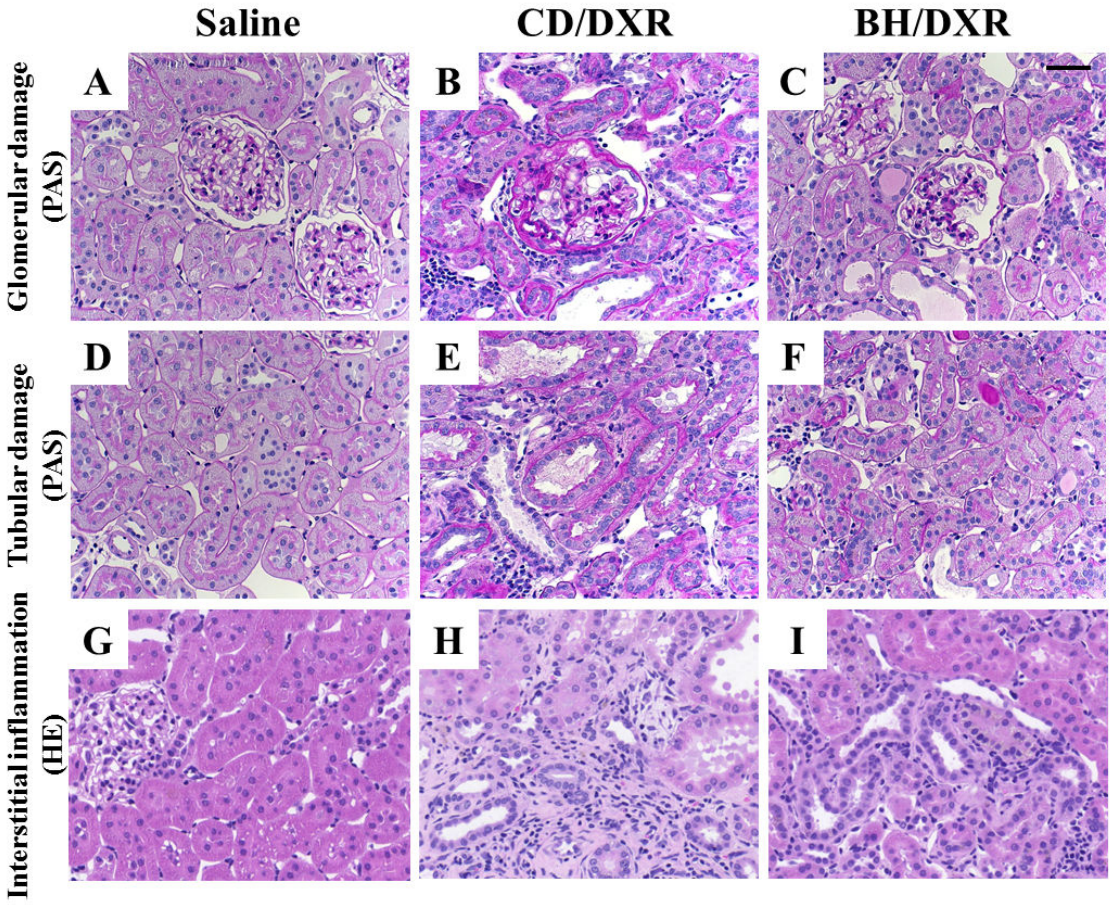

Figure 15: Renal histopathology

Top row (periodic acid–Schiff (PAS) staining) (A-C): Glomerular damage in the affected areas. Middle row (PAS staining) (D-F): Tubular damage in the affected areas. Lower row (hematoxylin-eosin (HE) staining) (G-I): Tubulointerstitial inflammatory infiltration.

Saline-injected control rats (A,D,G); CD-DXR: doxorubicin-injected CD rats (B,E,H); BH-DXR: doxorubicin-injected BH rats (C,F,I). Scale bar = 50 µm (C).

Table 2: Renal morphology: score values

CD: Charles Dawley rats, BH: Rowett, black hooded rats, /c: Saline-injected control rats, /DXR: Doxorubicin-injected rats. (dose: 5 mg/kg). n=8/group

Groups	Intact glomeruli (%)	Glomerulosclerosis score	Tubular score	Inflammation score
CD/DXR	36.3 ± 13.4	0.79 ± 0.22	2.01 ± 0.64	1.61 ± 0.32
BH/DXR	68.3 ± 8.4	0.32 ± 0.11	0.86 ± 0.44	1.06 ± 0.20
Control	93.3 ± 4.4	0.06 ± 0.04	0.00 ± 0.00	0.18 ± 0.06
P value (CD/DXR vs. BH/DXR)	<0.001	<0.001	<0.001	<0.01

5.2.6. Milder fibrosis was associated with less oxidative stress and inflammation in BH rats

Fibrosis was strikingly more intense in CD/DXR than in BH/DXR rats as demonstrated by Sirius red staining (Figure 16, A and B). Fibronectin immunostaining was detected only in 5.2±0.6% of the scanned areas in the saline-injected control groups, but increased significantly in the DXR-injected CD group. Significantly less fibronectin staining was detected in BH/DXR rats (Figure 17, A and B).

DOI:10.14753/SE.2018.1981

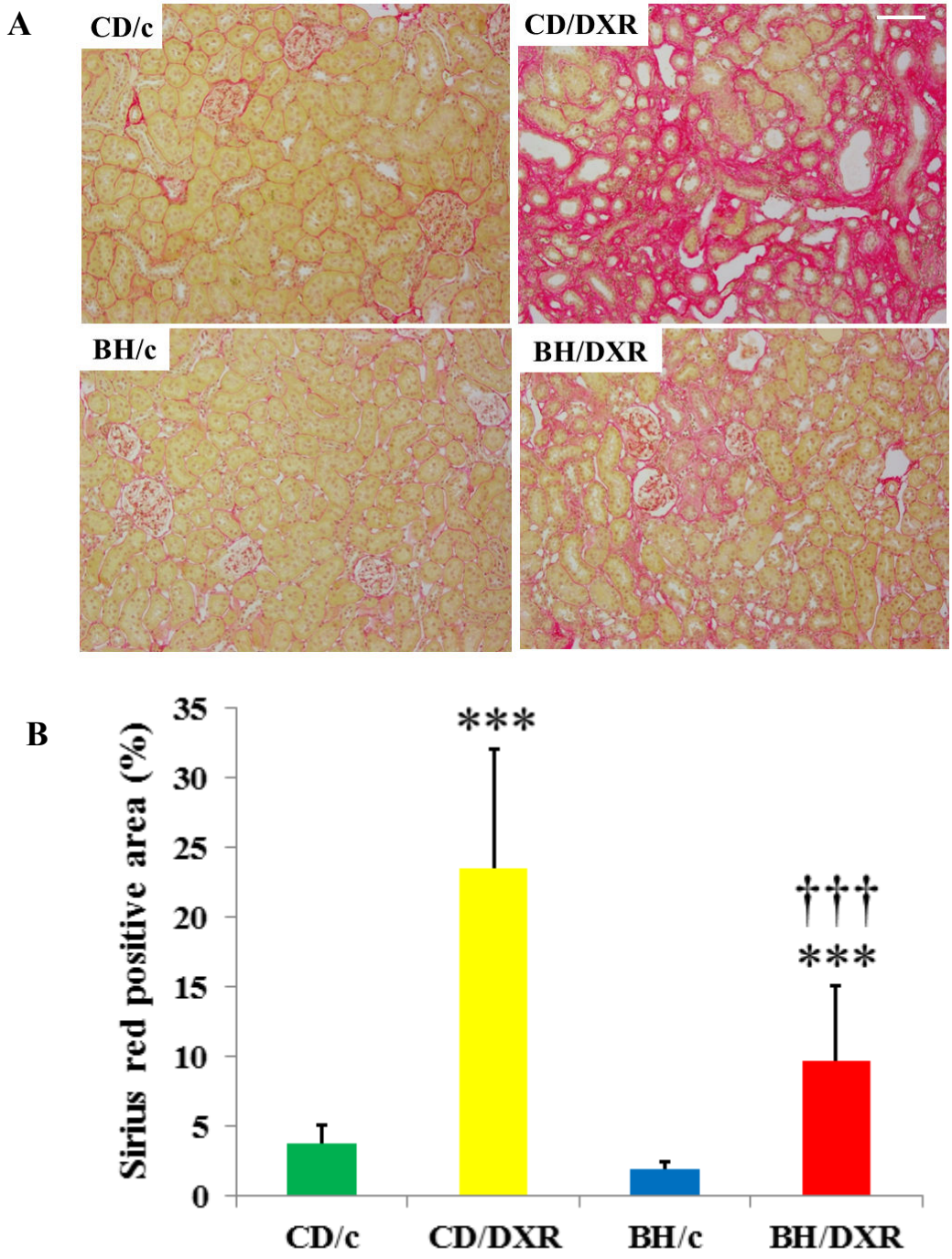

Figure 16: Sirius red staining (A) and computerized quantification of the stained areas (B)

CD: Charles Dawley rats, BH: Rowett, black hooded rats, /c: Saline-injected control rats, /DXR: Doxorubicin-injected rats. (dose: 5 mg/kg). n=8/group

*: $p<0.05$ vs. the control group of the same strain, †: $p<0.05$ vs. CD/DXR, control group. Scale bar = 100 µm.

DOI:10.14753/SE.2018.1981

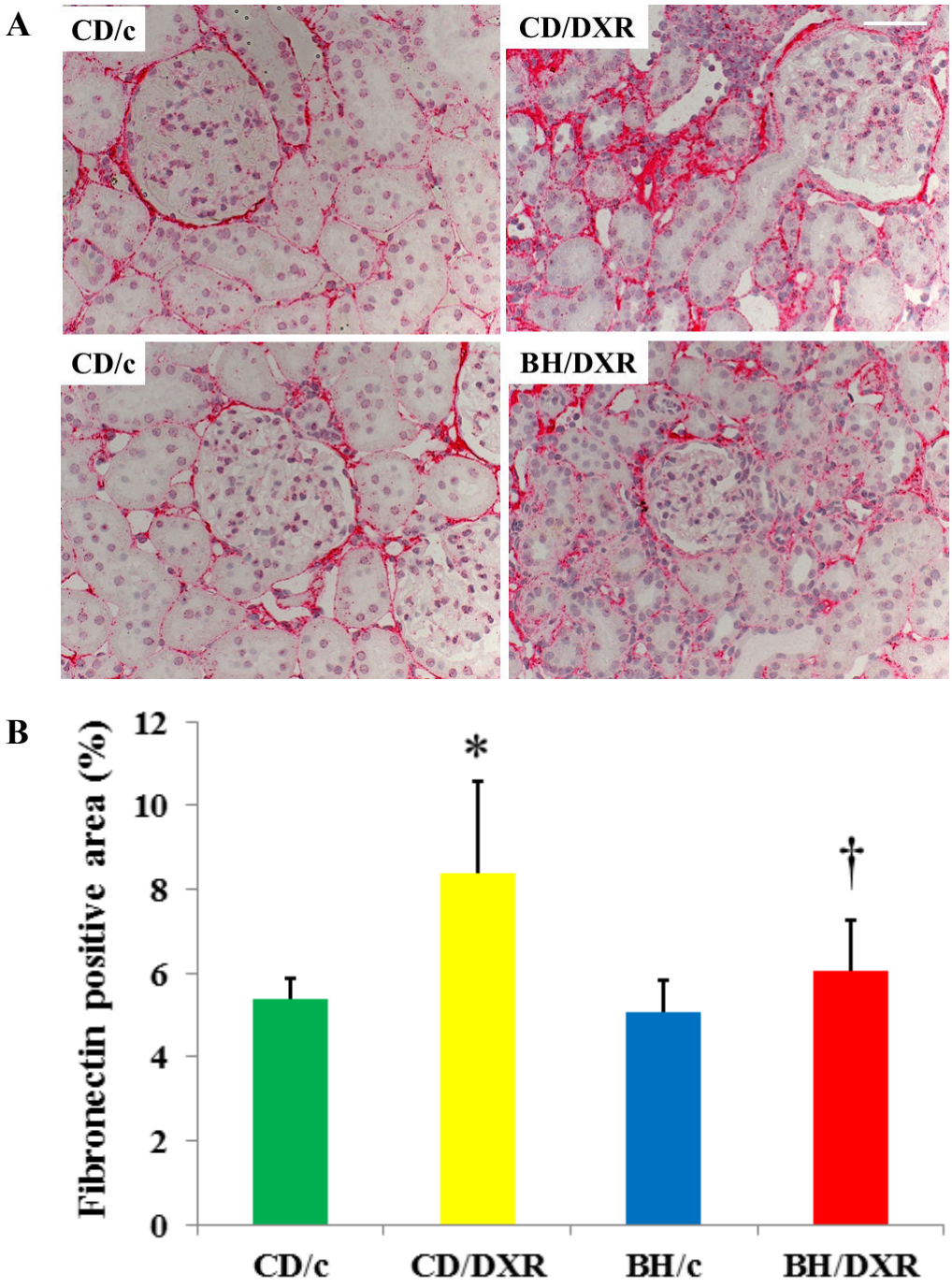

Figure 17: Fibronectin immunohistochemistry (A) and computerized quantification of the immunostained areas (B)

CD: Charles Dawley rats, BH: Rowett, black hooded rats, /c: Saline-injected control rats, /DXR: Doxorubicin-injected rats. (dose: 5 mg/kg). n=8/group

*: $p<0.05$ vs. the control group of the same strain, †: $p<0.05$ vs. CD/DXR, control group. Scale bar = 50 µm.

TGF-β1 and CTGF mRNA levels in the kidney cortex were not significantly different in the control groups compared to the DXR-injected BH rats, but were significantly elevated in the CD/DXR group (Figure 18, A and B). COL1A1 mRNA levels were elevated in the DXR-injected rats, but the elevation was significantly higher in the CD/DXR group (Figure 18, C).

Nephrin mRNA levels decreased in the kidney cortex of the CD/DXR group, but it was not reduced in the BH/DXR group (Figure 18, D), supporting a milder glomerular damage.

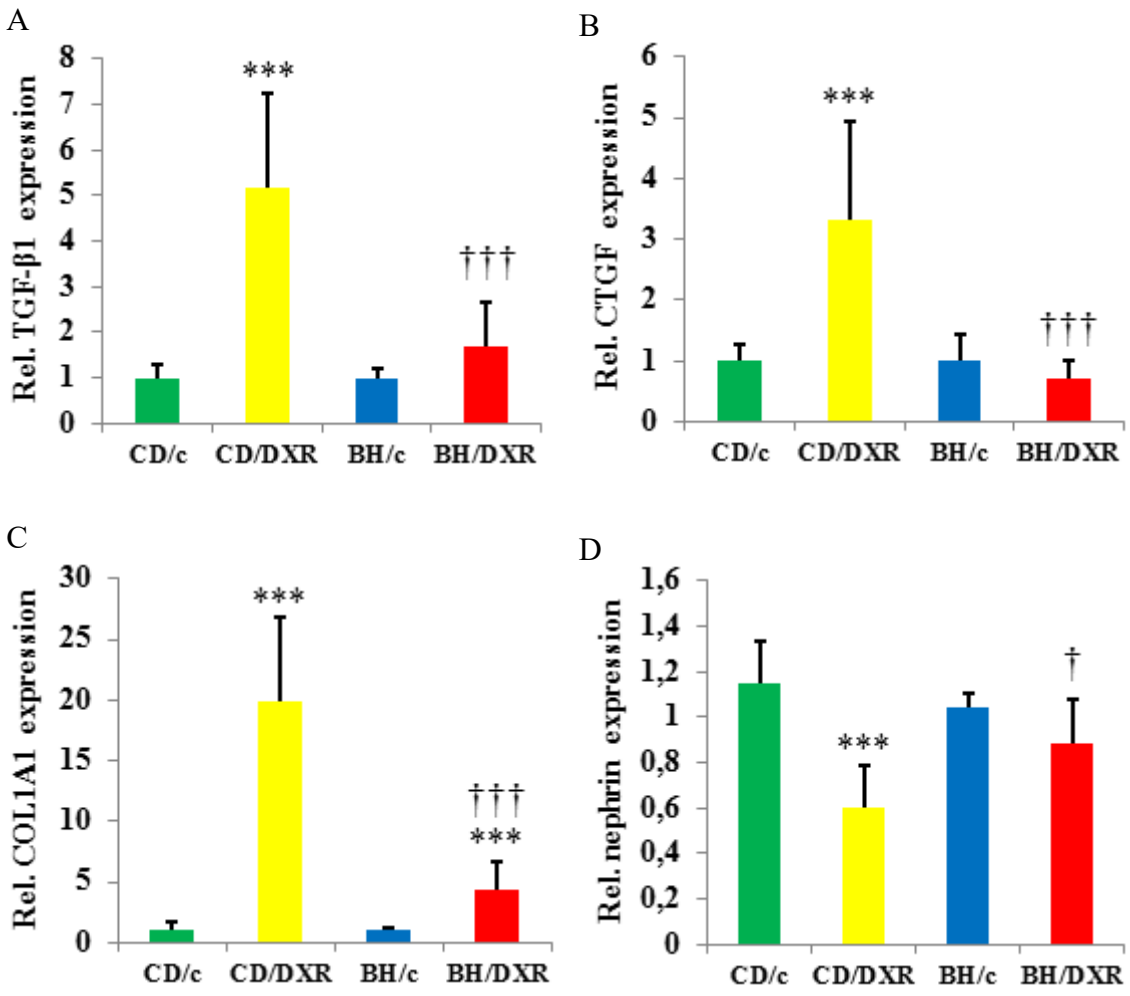

Figure 18: Renal cortical mRNA levels of fibrosis related markers.

A: TGF-β1, B: CTGF, C: COL1A1, D: nephrin. CD: CD rats, CD: Charles Dawley rats, BH: Rowett, black hooded rats, /c: Saline-injected control rats, /DXR: Doxorubicin-injected rats. (dose: 5 mg/kg). TGF-β1: transforming growth factor β1; CTGF: connective tissue growth factor; COL1A1: collagen type I alpha 1; **n**=8/group; *: $p<0.05$ vs. the control group of the same strain, †: $p<0.05$ vs. CD/DXR.

The mRNA levels of pro-inflammatory monocyte chemotactic protein 1 (MCP-1) (Figure 19, A) and pro-oxidant markers: p91phox and p47phox (Figure 19, B and C) increased in both DXR-injected groups; however the elevation was milder in the BH/DXR group.

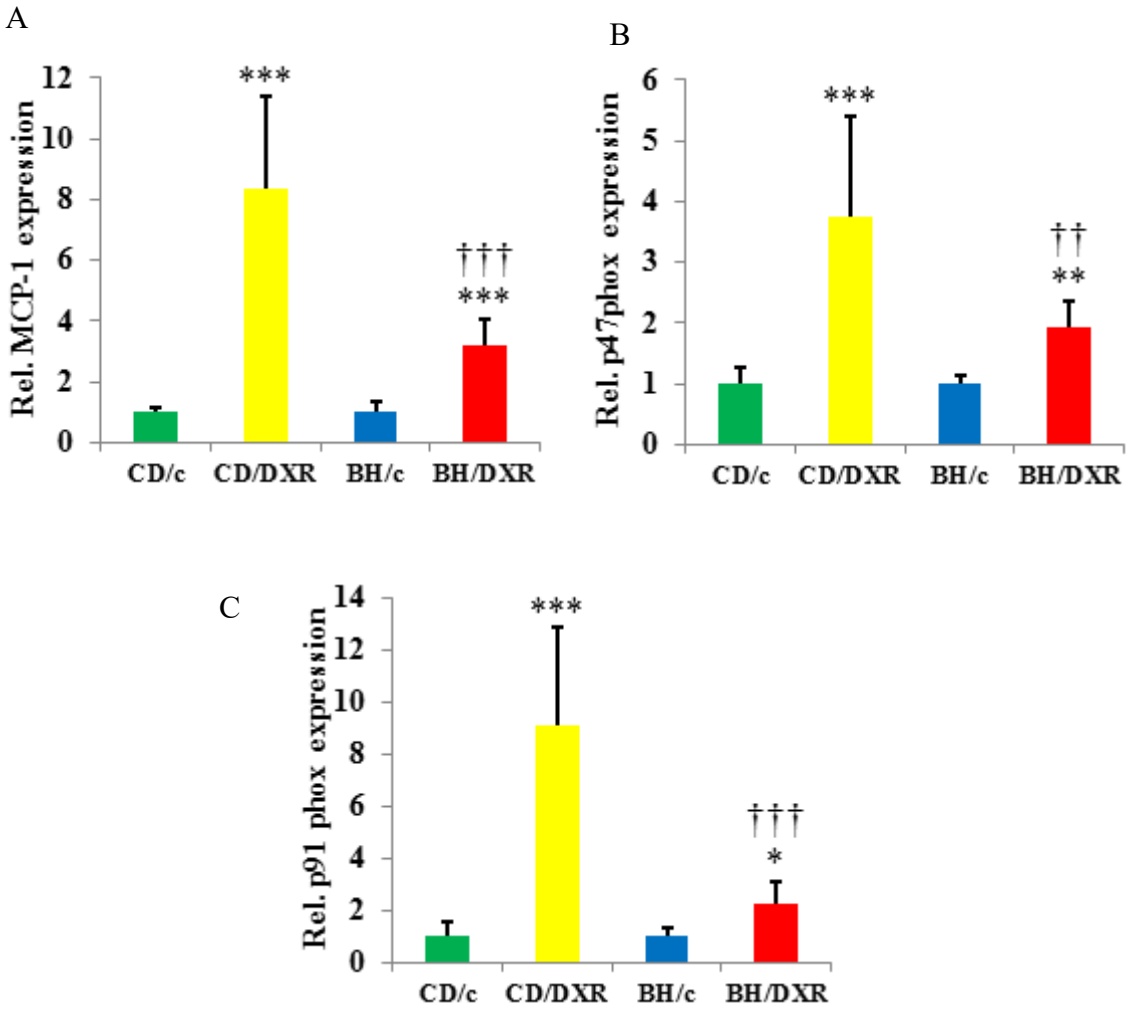

Figure 19: Renal cortical mRNA levels of inflammatory and oxidative markers.

A: MCP-1, B: p47phox, C: p91phox. CD: Charles Dawley rats, BH: Rowett, black hooded rats, /c: Saline-injected control rats, /DXR: Doxorubicin-injected rats. (dose: 5 mg/kg). MCP-1: monocyte chemotactic protein 1; p47phox: neutrophil cytosolic factor 1; p91phox: cytochrome b-245, beta polypeptide; **n**=8/group; *: $p<0.05$ vs. the control group of the same strain, †: $p<0.05$ vs. CD/DXR.

In the background of more severe kidney function deterioration demonstrated by proteinuria and fibrosis markers, severe lipid peroxidation and nitrative stress were detected in the kidneys of DXR-injected CD rats, while very mild changes were seen in the HNE or NT stained paraffin sections from the BH/DXR rats. Less staining was

DOI:10.14753/SE.2018.1981

corroborated by Western blot demonstrating significantly more renal HNE and NT in CD rats 8 weeks after DXR administration (Figure 20, 21).

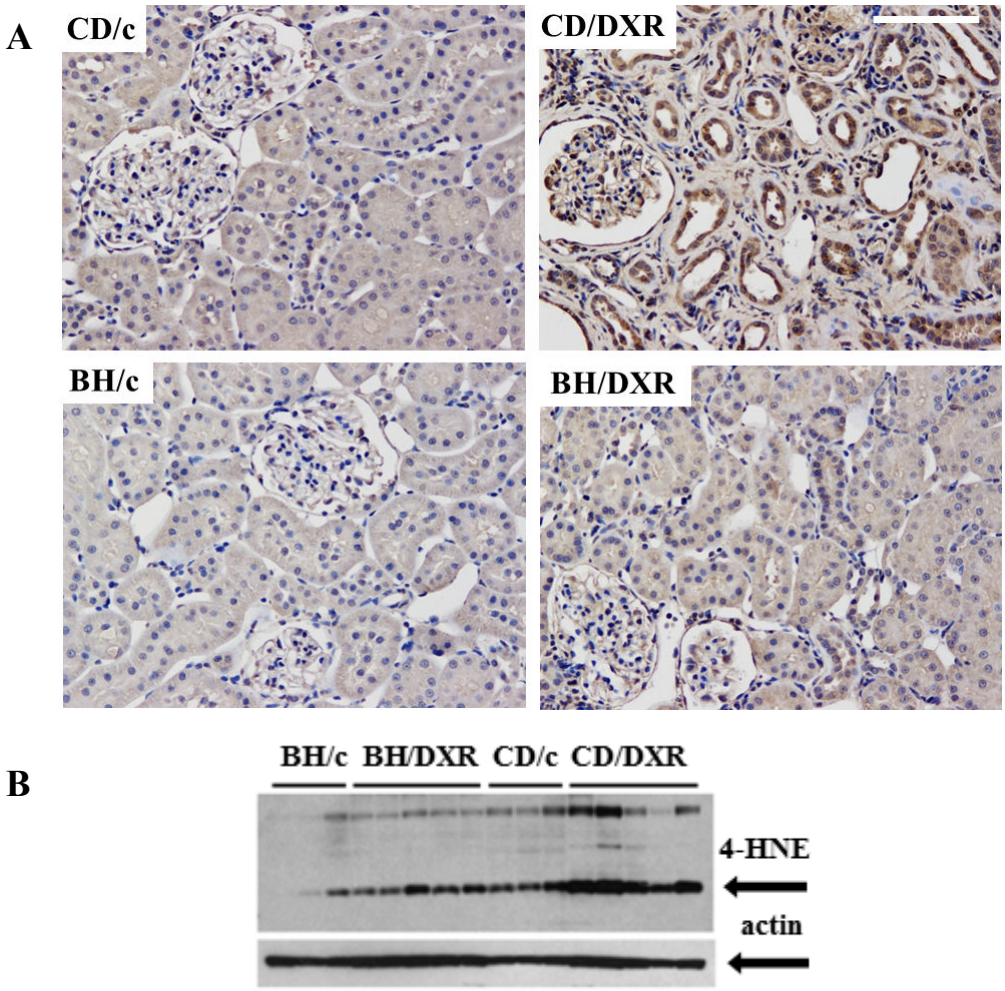

Figure 20: 4-hydrocy-2-nonenal (HNE) immunohistology (A) and quantification by Western blot (B).

CD: Charles Dawley rats, BH: Rowett, black hooded rats, /c: Saline-injected control rats, /DXR: Doxorubicin-injected rats (dose: 5 mg/kg). Scale bar = 100 µm.

DOI:10.14753/SE.2018.1981

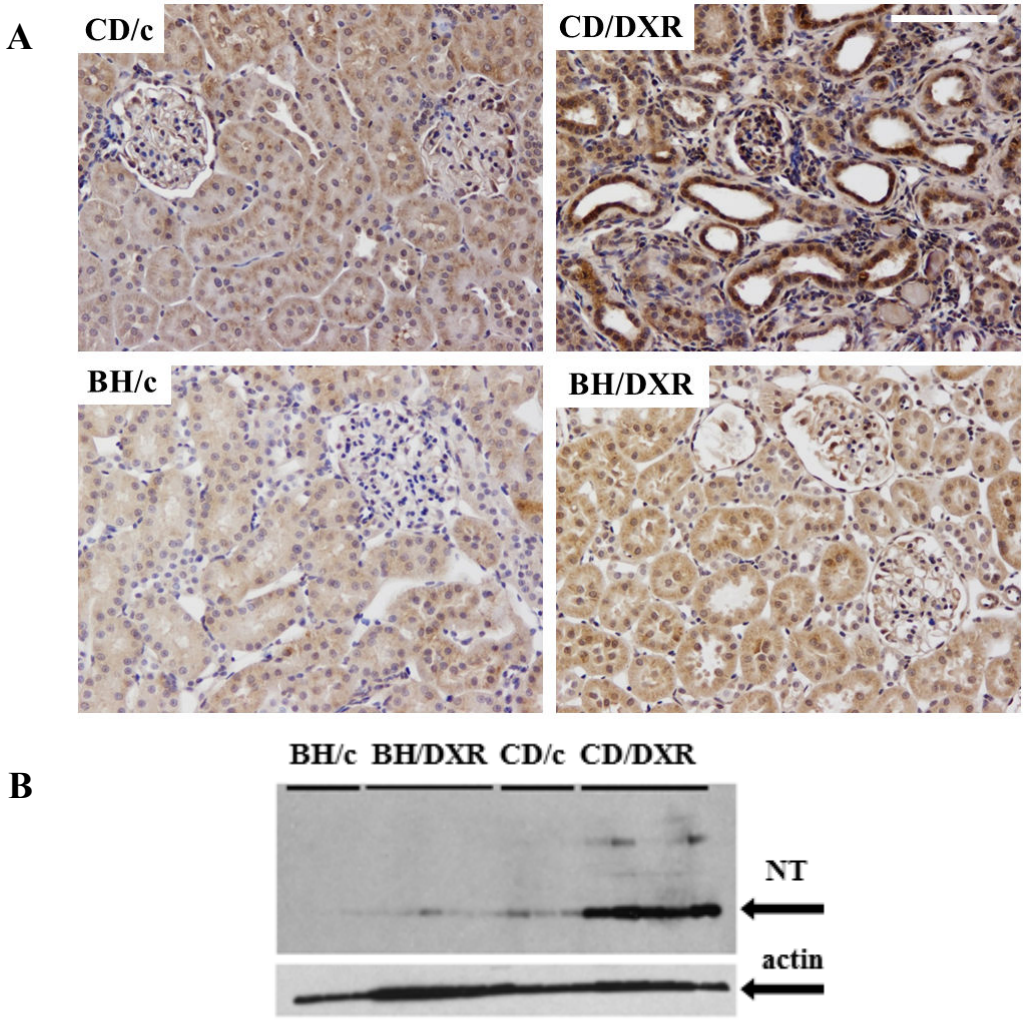

Figure 21: Nitrotyrosine (NT) immunohistology (A) and quantification by Western blot (B).
CD: Charles Dawley rats, BH: Rowett, black hooded rats, /c: Saline-injected control rats, /DXR: Doxorubicin-injected rats (dose: 5 mg/kg). Scale bar = 100 µm.

5.2.7. Tubulointerstitial fibrosis and inflammation were milder in DXR-injected BH vs. CD rats despite similar proteinuria

Urinary protein excretion and renal nephrin mRNA levels were similar in the two subgroups of CD and BH rats (BH/DXRp, CD/DXRp) with similar proteinuria (Table 3). Markers of fibrosis such as Sirius red staining and relative renal expression of TGF-β1, CTGF, COL1A1 were significantly lower in BH/DXRp rats. Paralleling less fibrosis, tubular damage detected by urinary NGAL excretion, markers of oxidative damage such as p47phox and p91phox expression and inflammation (MCP-1 expression) were significantly lower in BH/DXRp rats (Table 3).

DOI:10.14753/SE.2018.1981

Table 3: Comparison of doxorubicin-injected (DXR) Rowett, black hooded (BH) and Charles Dawley (CD) rats with similar proteinuria (BH/DXRp and CD/DXRp subgroups).

	CD/DXRp (n = 4)	BH/DXRp (n = 5)	P value
U Protein, week 8 (mg/24h)	396.5 ± 82.2	362.5 ± 30.3	0.42
Nephrin	0.68 ± 0.16	0.87 ± 0.19	0.19
U NGAL, week 8 (mg/24h)	10.1 ± 2.0	5.2 ± 1.6	<0.01
Sirius red (%)	18.0 ± 1.6	11.8 ± 1.0	<0.01
Fibronectin (%)	7.91 ± 2.45	5.55 ± 1.19	0.16
TGF-β1	6.00 ± 2.36	2.13 ± 1.23	<0.05
CTGF	3.71 ± 2.10	0.54 ± 0.11	<0.05
COL1A1	23.09 ± 6.14	5.79 ± 2.41	<0.01
p47phox	4.69 ± 1.51	1.95 ± 0.36	<0.05
p91phox	10.69 ± 2.47	1.94 ± 0.78	<0.01
MCP-1	9.23 ± 3.28	3.46 ± 0.99	<0.05

DOI:10.14753/SE.2018.1981

6. Discussion

6.1. Diabetic nephropathy study

Diabetic nephropathy is a devastating complication of diabetes and may ultimately progress to end-stage renal disease. The pathophysiological mechanisms of diabetic nephropathy have been under extensive study, and the results indicate an important role for podocyte injury in this process. We performed quantitative proteomic profiling of glomeruli isolated from rats with streptozotocin-induced diabetes and controls to identify differentially expressed proteins that could be associated with the development of podocyte injury. The major changes observed were among proteins involved in apoptosis, regulation of oxidative tolerance, and organization of the actin cytoskeleton, all processes known to be involved in podocyte function or injury and to participate in the development of diabetic nephropathy (115,116).

The cytoskeletal proteins down-regulated in the diabetic glomeruli included ezrin and its interaction partner, NHERF2. Ezrin and NHERF2 are important regulators of podocyte function because they link podocalyxin, the major sialoprotein of podocytes, to the actin cytoskeleton (40). However, the exact role of ezrin in podocyte injury in diabetic nephropathy has not been investigated before. In the nonphosphorylated, inactive conformation, the N- and C-termini of ezrin self-associate, but phosphorylation of threonine 567 leads to unfolding of the conformation, thus exposing the binding sites to F-actin and the plasma membrane, and activation of ezrin (117). Herein, we report that glomeruli of streptozotocin-injected rats show lower levels of total and, concomitantly, threonine 567 phosphorylated ezrin. We also found that the expression of ezrin is reduced in glomeruli of insulin-resistant and slightly diabetic obese Zucker rats and in podocytes of patients with type 2 diabetes without clinical nephropathy or histopathological signs of diabetic nephropathy. Supporting our findings, phosphorylation of ezrin has been reported to be reduced in skeletal muscle of obese patients with type 2 diabetes (118). These data together indicate that down-regulation of ezrin and/or its activity may be involved in the development of diabetic complications.

6.2. The toxic nephropathy study

Renal fibrosis is an intractable medical condition with high mortality and low quality of life. We present here an animal model useful to investigate the pathomechanisms of hereditary susceptibility or resistance to renal fibrosis in various kidney injury models (11,108,119). We demonstrated recently that BH rats were resistant to renal fibrosis with better preserved renal function and glomerular structure in a model of subtotal nephrectomy combined with salt and protein loading (96). In the present study we demonstrate that less oxidative/nitrative stress and inflammation was associated with slower progression of fibrosis in the resistant strain. Taken together with our previous report demonstrating similar resistance of BH vs. CD rats in the subtotal nephrectomy model, our present findings underline the pathophysiological relevance of inflammation and oxidative/nitrative stress pathways in fibrosis progression.

DXR nephropathy in rodents is a widely used experimental model of human FSGS. (72,120) Direct exposure of the kidneys to DXR is a requirement for the development of podocyte injury in rats, as clipping the renal artery during DXR injection prevents nephropathy (120). A single intravenous injection with 4–7,5 mg/kg DXR led to well predictable deterioration of glomerular structure, proteinuria, tubular and interstitial inflammation culminating in renal fibrosis in fibrosis-sensitive Sprague Dawley or Wistar rats (121). Glomerular structural changes develop in a well predictable manner: altered mRNA levels of nephrin, podocin and NEPH1, and swelling of the foot-processes are present at day 7 (122). Podocyte swelling with cytoplasmic vesicles appear at day 14, and finally, widespread podocyte foot process fusion at day 28 (92). As a marker of glomerular filtration barrier damage, proteinuria develops (123). Repeated low dose DXR has been widely used to induce toxic cardiomyopathy. In our model cardiac toxicity was absent after a single DXR injection, as demonstrated by the lack of changes in histology or the sensitive cardiomyopathy marker Cx-43.

BH rats have a slower growth rate than age matched CD rats under healthy circumstances. The body weight curves in control animals of our study were similar to the previous findings (124,125). In our study, sensitive CD rats developed significant and progressive proteinuria starting two weeks after administration of 5 mg/kg DXR

similarly to that shown in previous publications (92,122-126). Nephrin plays an important role in maintaining the structural integrity and the functional soundness of the slit diaphragm (127). Significant nephrin loss was demonstrated in CD rats in the background of the proteinuria. The severity of proteinuria was milder and progression was slower in BH rats. Thus, as BH rats had similar nephrin mRNA levels to that in the control rats of the same strain, nephrin might play a central role in the progression of DXR-induced fibrosis. Proteinuria-associated interstitial fibrosis and tubular atrophy (IFTA) has been recognized previously (128). Podocyte dysfunction and consequent proteinuria has been recently reinforced as a major determinant of tubular injury, inflammation and apoptosis leading to progressive IFTA (129). According to our present study and previous literature (130) IFTA developed as part of DXR nephropathy. Urinary NGAL excretion is a sensitive marker of tubular damage not only during acute kidney injury (131,132), but also during IFTA (133). In our study, significantly less proteinuria was accompanied by reduced tubular damage and less urinary NGAL excretion after injection with DXR in the BH than in the CD strain. Similarly, less renal damage and less proteinuria was accompanied by better maintained body weight and significantly prolonged survival in BH rats. These data support that IFTA is secondary to proteinuria in the DXR model. The single administration of DXR and consequent albuminuria led to tubulointerstitial inflammation and fibrosis demonstrated by PAS, Sirius red and fibronectin and collagen synthesis and the presence of the pro-fibrotic transforming growth factor (TGF-β1) (134,135), and its downstream mediator connective tissue growth factor (CTGF) (136). Significant reduction of these fibrotic pathways in the resistant BH strain underlines the relevance of the TGF-β1-CTGF cascade-mediated matrix deposition in the development of DXR-induced renal fibrosis (Figure 22).

DOI:10.14753/SE.2018.1981

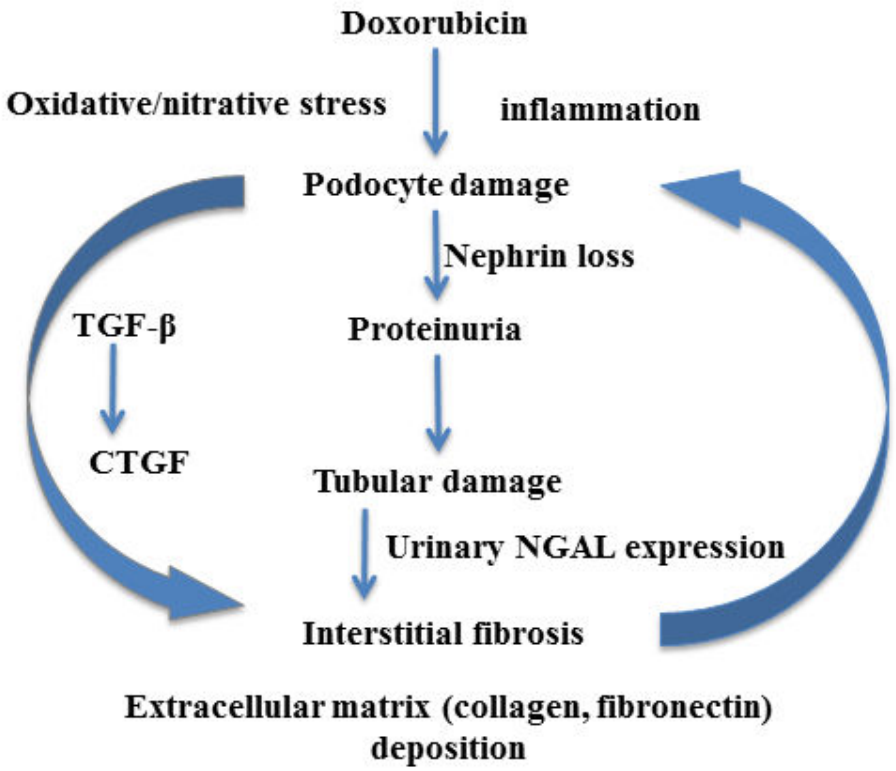

Figure 22: Suggested mechanisms of doxorubicin induced nephropathy.

A single administration of doxorubicin induced podocyte damage demonstrated by loss of nephrin and leading to proteinuria. Proteinuria damages tubules as demonstrated by increased urinary NGAL excretion. Tubular damage leads to interstitial inflammation and fibrosis with collagen and fibronectin deposition. Inflammation is accompanied by oxidative/nitrative damage triggering further immune activation. Reverse arrows symbolize main elements of the vicious circle. Sustained injury activates the TGF-β1 and CTGF profibrotic axis. Sustained injury eventually leads to fibrotic end-stage kidney. NGAL: neutrophil gelatinase-associated lipocalin; TGF-β1: transforming growth factor β1; CTGF: connective tissue growth factor.

Oxidative and nitrative stress has been proposed as the mechanism by which DXR induces glomerular toxicity in rats. Redox cycling of the quinone functional group of DXR was proposed as the key factor in DXR nephrotoxicity (84). Reactive oxygen species (ROS) may initiate a degenerative cascade by the oxidation of cellular thiols and lipid membrane structures (137). DXR has been suggested to upregulate NADPH-oxidase (NOX), an important source of ROS in the kidney (86). However, the role of oxidative mechanisms in DXR toxicity has been questioned as well (138). In our study, signs of lipid peroxidation and nitrative stress were milder in the BH rats, compared to

those in CD rats suggesting that less oxidative and nitrative stress may be responsible, at least in part, for the resistance of BH rats against renal fibrosis. This observation supports the role of oxidative and nitrative mechanisms in DXR toxicity.

Our results obtained in the subgroups of DXR-injected CD and BH rats with similar urinary protein excretion support our view that BH rats are less susceptible to tubulointerstitial fibrosis induced by proteinuria. Renal nephrin mRNA expression was similar in the two subgroups, suggesting that the degree of podocyte injury and slit diaphragm leakiness is a primary determinant of proteinuria independent of the genetic background. However, despite similar proteinuria, most markers of renal fibrosis, oxidative stress and inflammation were significantly lower in BH rats. These results support the role of inflammation in proteinuria-induced tubulointerstitial fibrosis.

Resistance mechanisms against DXR nephropathy were studied previously in rat (139) and mouse (140) strains. In spontaneously hypertensive (SHR) rats, cardio- and nephrotoxicity of DXR was more severe than in congenic Wistar-Kyoto (WKY), similarly to SHR-heart failure rats after subsequent administration of 2 mg/kg DXR on 8 consecutive days. Twelve weeks after the last dose of DXR renal lesions were similar to those in our study including podocyte adhesion leading to glomerulosclerosis and mononuclear infiltration, tubular atrophy and fibrotic matrix expansion in the tubulointerstitium (139). Severity of these histological changes correlated with strain sensitivity. Similarly to our study, strain differences were partially explained by a difference in the severity of inflammation and arachidonic acid metabolism. Sensitivity to DXR nephropathy was investigated previously in fibrosis-resistant C57BL/6 and -sensitive BALB/c mice (11). The difference in susceptibility was attributed to a mutation in the PRKDC gene encoding the catalytic subunit of a DNA activated protein kinase (DNA-PK), a double stranded break repair protein (11,141). This mutation is also responsible for the severe combined immunodeficiency phenotype in mice and rats (142). DNA-PK expression and activity was also profoundly lower in BALB/c than in C57BL/6 mice in a radiation-induced apoptosis model (143). Thus, DNA-PK seems to be crucial in toxic injury models. As inflammation and related oxidative stress also induces DNA damage, the PRKDC gene may play an important role also in our model.

DOI:10.14753/SE.2018.1981

Fibrosis is mediated by myofibroblasts activated by TGF-β1, MCP-1, etc. (144). In our study, decreased MCP-1 mRNA levels were found in resistant BH rats, which is one of the key chemokines for the migration and infiltration of macrophages to sites of inflammation (145). The mRNA levels of p91phox, also known as NADPH oxidase 2 (NOX2) were also lower in BH rats. NOX2 plays an important role in ROS production of phagocytes and T cells. Furthermore, the mRNA level of p47phox, which plays a role in the activation of the NOX2/p22phox complex in the membrane of phagocytes (146), was also milder in BH rats. These findings suggest that less inflammation, accompanied by milder ROS production of the neutrophil cells and macrophages may play a role in the resistance of BH rats against DXR nephropathy.

DOI:10.14753/SE.2018.1981

7. Conclusions

Diabetic nephropathy is a serious complication of DM, and despite the extensive investigations of this disease, there are very few options for specific treatment.
Fluorescence-based two-dimensional difference gel electrophoresis, coupled with mass spectrometry, identified 29 differentially expressed spots, including the actin-binding protein ezrin, and its interaction partner, NHERF2, which were down-regulated in streptozotocin-injected rats. Not just the total amount, but the active, phosphorylated ezrin was also reduced in diabetic SD rats. Podocalyxin is connected to actin through ezrin/NHERF2 complex, and it was down-regulated in STZ-induced diabetic SD rats. Ezrin expression was also lower in obese, diabetic Zucker rats and in human patients with diabetes. In conclusion, our data suggest that down-regulation of ezrin may associate with the development of the kidney complication in diabetes.

In our toxic nephropathy study, BH rats were resistant to renal fibrosis compared to CD rats. Fibrosis sensitive CD rats developed progressive proteinuria after DXR injection, with significant loss of nephrin, and FSGS-like histological lesions. DXR-injected BH rats had similar nephrin mRNA levels to that in the control rats of the same strain, with milder proteinuria and less severe glomerular changes. Consequent proteinuria contributed to the development of interstitial fibrosis and tubular atrophy. BH rats had reduced urinary NGAL excretion, accompanied by milder signs of tubulointerstitial inflammation and fibrosis, with less severe signs of lipid peroxidation and protein nitrosylation. Interestingly, markers of tubular atrophy, interstitial fibrosis, oxidative- and nitrative stress were milder in BH rats even with similar levels of proteinuria. BH rats also had prolonged survival. In conclusion, resistance of BH rats against renal fibrosis highlighted the role of inflammation induced oxidative/nitrative stress in chronic podocyte injury leading to glomerulosclerosis and consequent proteinuria in DXR nephropathy.

DOI:10.14753/SE.2018.1981

8. Summary

Chronic kidney disease (CKD) is a major healthcare problem with high prevalence both in Europe and in the US. CKD slowly progresses to end-stage renal disease (ESRD), independently from the primary insult. The pathologic manifestation of CKD is renal fibrosis.

Diabetic nephropathy is a complication of diabetes and a major cause of end-stage renal disease. To characterize the early pathophysiological mechanisms leading to glomerular podocyte injury in diabetic nephropathy, we performed quantitative proteomic profiling of glomeruli isolated from rats with streptozotocin-induced diabetes and controls. The actin-binding proteins ezrin and NHERF2 were down-regulated in the streptozotocin group. The podocalyxin, an important element of the slit diaphragm, was also reduced in streptozotocin-injected rats. Ezrin expression was also lower in patients with diabetes. These findings suggest that the cytoskeletal protein: ezrin is involved in the development of diabetic nephropathy.

Genetic background has a strong influence on the progression of chronic renal fibrosis. We recently found that Rowett black hooded rats (BH) were resistant to renal fibrosis induced by subtotal nephrectomy plus salt and protein loading. We investigated the nature of this resistance using a podocyte specific injury caused by Doxorubicin.

In comparison to the fibrosis-sensitive, Charles Dawley rats, the BH rats had longer survival, milder proteinuria and lesstubular damage, glomerulosclerosis, tubulointerstitial fibrosis and matrix deposition. Less fibrosis was associated with reduced mRNA levels of profibrotic factors. Milder inflammation demonstrated by histology was confirmed by less monocyte chemotactic protein 1 (MCP-1) mRNA. As a consequence of less inflammation, reduced oxidative enzyme expression was detected accompanied by less lipid peroxidation and less protein nitrosylation demonstrated by immunohistochemistry and quantified by Western blot. Our results demonstrate that mediators of fibrosis, inflammation and oxidative/nitrative stress were suppressed in fibrosis-resistant Rowett black hooded rats, underlying the importance of these pathomechanisms in the progression of chronic kidney disease.

DOI:10.14753/SE.2018.1981

Összefoglalás

A krónikus veseelégtelenség gyakori, súlyos kórkép, amely vesefibrózishoz és végstádiumú vesebetegséghez vezet. A végstádiumú vesebetegség kialakulásának leggyakoribb oka a cukorbetegség. A diabéteszes nefropátia glomeruláris elváltozásainak vizsgálatához streptozotocinnal injektált cukorbeteg-, és citrát pufferrel injektált egészséges kontroll patkányok veséit hasonlítottuk össze izolált glomerulusok kvantitatív proteomikai vizsgálatával. Eredményeink az aktin-kötő fehérjék közül az ezrin és az NHERF2 expressziójának csökkenését mutatták a cukorbeteg állatokban. Velük együtt a podocalyxin-nak, a résmembrán egyik fontos elemének az expressziója is csökkent a streptozotocinnal injektált patkányokban. Az ezrin-expresszió csökkenése cukorbeteg páciensek nefrektómiás szövetmintáiban is megfigyelhető volt. Eredményeink rámutatnak a citoszkeleton fehérje: ezrin szerepére a diabéteszes nefropátia kialakulása során.

A genetikai háttér fontos szerepet játszik a vesefibrózis kialakulásában. Korábbi vizsgálatainkban a Rowett csuklyás patkányok (black hooded, BH) ellenállóak voltak a vesefibrózis só- és fehérjeterheléssel kombinált szubtotális nefrektómia állatmodelljével szemben. Ennek a rezisztenciának a hátterét vizsgáltuk doxorubicin nefropátia modellen. A vesefibrózisra érzékeny Charles Dawley (CD) patkányokkal összehasonlítva a BH patkányok Doxorubicin adagolás után jobb túlélést, enyhébb proteinuriát, glomeruláris és tubuláris károsodást, kevesebb kötőszövet-felhalmozódást és profibrotikus faktor expressziót mutattak. Az enyhébb gyulladásos infiltráció és az alacsonyabb MCP-1 mRNS szint enyhébb gyulladást igazolt, amit a reaktív szabadgyökök termeléséért felelős enzimek expressziójának csökkenése kísért, következményesen kisebb mértékű oxidatív károsodással. Eredményeink alátámasztják a fibrotikus és gyulladásos faktorok, valamint az oxidatív/nitratív stressz szerepét a vesefibrózis progressziójában és a BH állatok rezisztenciájában.

9. Bibliography

1. Comas J, Arcos E, Castell C, Cases A, Martinez-Castelao A, Donate T, Esmatjes E (2013) Evolution of the incidence of chronic kidney disease Stage 5 requiring renal replacement therapy in the diabetic population of Catalonia. Nephrol Dial Transplant 28: 1191-1198.
2. (2014) National Chronic Kidney Disease Fact Sheet. Available: http://wwwcdcgov/diabetes/pubs/factsheets/kidneyhtm.
3. Pourghasem M, Shafi H, Babazadeh Z (2015) Histological changes of kidney in diabetic nephropathy. Caspian J Intern Med 6: 120-127.
4. Saran R, Li Y, Robinson B, Abbott KC, Agodoa LY, Ayanian J, Bragg-Gresham J, Balkrishnan R, Chen JL, Cope E, Eggers PW, Gillen D, Gipson D, Hailpern SM, Hall YN, He K, Herman W, Heung M, Hirth RA, Hutton D, Jacobsen SJ, Kalantar-Zadeh K, Kovesdy CP, Lu Y, Molnar MZ, Morgenstern H, Nallamothu B, Nguyen DV, O'Hare AM, Plattner B, Pisoni R, Port FK, Rao P, Rhee CM, Sakhuja A, Schaubel DE, Selewski DT, Shahinian V, Sim JJ, Song P, Streja E, Kurella Tamura M, Tentori F, White S, Woodside K, Hirth RA (2016) US Renal Data System 2015 Annual Data Report: Epidemiology of Kidney Disease in the United States. Am J Kidney Dis 67: A7-8.
5. Macconi D, Remuzzi G, Benigni A (2014) Key fibrogenic mediators: old players. Renin-angiotensin system. Kidney Int Suppl (2011) 4: 58-64.
6. Cameron JS (1996) The enigma of focal segmental glomerulosclerosis. Kidney Int Suppl 57: S119-131.
7. Fitzgibbon WR, Greene EL, Grewal JS, Hutchison FN, Self SE, Latten SY, Ullian ME (1999) Resistance to remnant nephropathy in the Wistar-Furth rat. J Am Soc Nephrol 10: 814-821.
8. Fleck C, Appenroth D, Jonas P, Koch M, Kundt G, Nizze H, Stein G (2006) Suitability of 5/6 nephrectomy (5/6NX) for the induction of interstitial renal fibrosis in rats--influence of sex, strain, and surgical procedure. Exp Toxicol Pathol 57: 195-205.
9. Rostand SG, Kirk KA, Rutsky EA, Pate BA (1982) Racial differences in the incidence of treatment for end-stage renal disease. N Engl J Med 306: 1276-1279.

10. Kaplan JM, Kim SH, North KN, Rennke H, Correia LA, Tong HQ, Mathis BJ, Rodriguez-Perez JC, Allen PG, Beggs AH, Pollak MR (2000) Mutations in ACTN4, encoding alpha-actinin-4, cause familial focal segmental glomerulosclerosis. Nat Genet 24: 251-256.
11. Papeta N, Chan KT, Prakash S, Martino J, Kiryluk K, Ballard D, Bruggeman LA, Frankel R, Zheng Z, Klotman PE, Zhao H, D'Agati VD, Lifton RP, Gharavi AG (2009) Susceptibility loci for murine HIV-associated nephropathy encode trans-regulators of podocyte gene expression. J Clin Invest 119: 1178-1188.
12. Leeuwis JW, Nguyen TQ, Dendooven A, Kok RJ, Goldschmeding R (2010) Targeting podocyte-associated diseases. Adv Drug Deliv Rev 62: 1325-1336.
13. Kavvadas P, Dussaule JC, Chatziantoniou C (2014) Searching novel diagnostic markers and targets for therapy of CKD. Kidney Int Suppl (2011) 4: 53-57.
14. Reiser J, von Gersdorff G, Loos M, Oh J, Asanuma K, Giardino L, Rastaldi MP, Calvaresi N, Watanabe H, Schwarz K, Faul C, Kretzler M, Davidson A, Sugimoto H, Kalluri R, Sharpe AH, Kreidberg JA, Mundel P (2004) Induction of B7-1 in podocytes is associated with nephrotic syndrome. J Clin Invest 113: 1390-1397.
15. D'Agati VD (2008) Podocyte injury in focal segmental glomerulosclerosis: Lessons from animal models (a play in five acts). Kidney Int 73: 399-406.
16. Wharram BL, Goyal M, Wiggins JE, Sanden SK, Hussain S, Filipiak WE, Saunders TL, Dysko RC, Kohno K, Holzman LB, Wiggins RC (2005) Podocyte depletion causes glomerulosclerosis: diphtheria toxin-induced podocyte depletion in rats expressing human diphtheria toxin receptor transgene. J Am Soc Nephrol 16: 2941-2952.
17. Wasik AA, Koskelainen S, Hyvonen ME, Musante L, Lehtonen E, Koskenniemi K, Tienari J, Vaheri A, Kerjaschki D, Szalay C, Revesz C, Varmanen P, Nyman TA, Hamar P, Holthofer H, Lehtonen S (2014) Ezrin is down-regulated in diabetic kidney glomeruli and regulates actin reorganization and glucose uptake via GLUT1 in cultured podocytes. Am J Pathol 184: 1727-1739.
18. Szalay CI, Erdelyi K, Kokeny G, Lajtar E, Godo M, Revesz C, Kaucsar T, Kiss N, Sarkozy M, Csont T, Krenacs T, Szenasi G, Pacher P, Hamar P (2015) Oxidative/Nitrative Stress and Inflammation Drive Progression of Doxorubicin-

Induced Renal Fibrosis in Rats as Revealed by Comparing a Normal and a Fibrosis-Resistant Rat Strain. PLoS One 10: e0127090.

19. Conserva F, Gesualdo L, Papale M (2016) A Systems Biology Overview on Human Diabetic Nephropathy: From Genetic Susceptibility to Post-Transcriptional and Post-Translational Modifications. J Diabetes Res 2016: 7934504.
20. Najafian B, Fogo AB, Lusco MA, Alpers CE (2015) AJKD Atlas of Renal Pathology: diabetic nephropathy. Am J Kidney Dis 66: e37-38.
21. Kanwar YS, Sun L, Xie P, Liu FY, Chen S (2011) A glimpse of various pathogenetic mechanisms of diabetic nephropathy. Annu Rev Pathol 6: 395-423.
22. Mazzucco G, Bertani T, Fortunato M, Bernardi M, Leutner M, Boldorini R, Monga G (2002) Different patterns of renal damage in type 2 diabetes mellitus: a multicentric study on 393 biopsies. Am J Kidney Dis 39: 713-720.
23. Alsaad KO, Herzenberg AM (2007) Distinguishing diabetic nephropathy from other causes of glomerulosclerosis: an update. J Clin Pathol 60: 18-26.
24. Reddy GR, Kotlyarevska K, Ransom RF, Menon RK (2008) The podocyte and diabetes mellitus: is the podocyte the key to the origins of diabetic nephropathy? Curr Opin Nephrol Hypertens 17: 32-36.
25. Hostetter TH, Rennke HG, Brenner BM (1982) The case for intrarenal hypertension in the initiation and progression of diabetic and other glomerulopathies. Am J Med 72: 375-380.
26. Bhatti AB, Usman M (2015) Drug Targets for Oxidative Podocyte Injury in Diabetic Nephropathy. Cureus 7: e393.
27. Forbes JM, Cooper ME, Oldfield MD, Thomas MC (2003) Role of advanced glycation end products in diabetic nephropathy. J Am Soc Nephrol 14: S254-258.
28. Kwoh C, Shannon MB, Miner JH, Shaw A (2006) Pathogenesis of nonimmune glomerulopathies. Annu Rev Pathol 1: 349-374.
29. Wolf G, Chen S, Ziyadeh FN (2005) From the periphery of the glomerular capillary wall toward the center of disease: podocyte injury comes of age in diabetic nephropathy. Diabetes 54: 1626-1634.
30. Flyvbjerg A, Dagnaes-Hansen F, De Vriese AS, Schrijvers BF, Tilton RG, Rasch R (2002) Amelioration of long-term renal changes in obese type 2 diabetic mice by a neutralizing vascular endothelial growth factor antibody. Diabetes 51: 3090-3094.

31. Nakagawa T, Sato W, Glushakova O, Heinig M, Clarke T, Campbell-Thompson M, Yuzawa Y, Atkinson MA, Johnson RJ, Croker B (2007) Diabetic endothelial nitric oxide synthase knockout mice develop advanced diabetic nephropathy. J Am Soc Nephrol 18: 539-550.
32. Welsh GI, Hale LJ, Eremina V, Jeansson M, Maezawa Y, Lennon R, Pons DA, Owen RJ, Satchell SC, Miles MJ, Caunt CJ, McArdle CA, Pavenstadt H, Tavare JM, Herzenberg AM, Kahn CR, Mathieson PW, Quaggin SE, Saleem MA, Coward RJ (2010) Insulin signaling to the glomerular podocyte is critical for normal kidney function. Cell Metab 12: 329-340.
33. Coward RJ, Welsh GI, Yang J, Tasman C, Lennon R, Koziell A, Satchell S, Holman GD, Kerjaschki D, Tavare JM, Mathieson PW, Saleem MA (2005) The human glomerular podocyte is a novel target for insulin action. Diabetes 54: 3095-3102.
34. Mathieson PW (2012) The podocyte cytoskeleton in health and in disease. Clin Kidney J 5: 498-501.
35. Arpin M, Algrain M, Louvard D (1994) Membrane-actin microfilament connections: an increasing diversity of players related to band 4.1. Curr Opin Cell Biol 6: 136-141.
36. Vaheri A, Carpen O, Heiska L, Helander TS, Jaaskelainen J, Majander-Nordenswan P, Sainio M, Timonen T, Turunen O (1997) The ezrin protein family: membrane-cytoskeleton interactions and disease associations. Curr Opin Cell Biol 9: 659-666.
37. Tsukita S, Yonemura S (1999) Cortical actin organization: lessons from ERM (ezrin/radixin/moesin) proteins. J Biol Chem 274: 34507-34510.
38. Kurihara H, Anderson JM, Farquhar MG (1995) Increased Tyr phosphorylation of ZO-1 during modification of tight junctions between glomerular foot processes. Am J Physiol 268: F514-524.
39. Hugo C, Nangaku M, Shankland SJ, Pichler R, Gordon K, Amieva MR, Couser WG, Furthmayr H, Johnson RJ (1998) The plasma membrane-actin linking protein, ezrin, is a glomerular epithelial cell marker in glomerulogenesis, in the adult kidney and in glomerular injury. Kidney Int 54: 1934-1944.
40. Takeda T, McQuistan T, Orlando RA, Farquhar MG (2001) Loss of glomerular foot processes is associated with uncoupling of podocalyxin from the actin cytoskeleton. J Clin Invest 108: 289-301.

41. McRobert EA, Gallicchio M, Jerums G, Cooper ME, Bach LA (2003) The amino-terminal domains of the ezrin, radixin, and moesin (ERM) proteins bind advanced glycation end products, an interaction that may play a role in the development of diabetic complications. J Biol Chem 278: 25783-25789.
42. Macdougall IC, Bircher AJ, Eckardt KU, Obrador GT, Pollock CA, Stenvinkel P, Swinkels DW, Wanner C, Weiss G, Chertow GM, Conference P (2016) Iron management in chronic kidney disease: conclusions from a "Kidney Disease: Improving Global Outcomes" (KDIGO) Controversies Conference. Kidney Int 89: 28-39.
43. Izquierdo MJ, Cavia M, Muniz P, de Francisco AL, Arias M, Santos J, Abaigar P (2012) Paricalcitol reduces oxidative stress and inflammation in hemodialysis patients. BMC Nephrol 13: 159.
44. Schleicher E, Friess U (2007) Oxidative stress, AGE, and atherosclerosis. Kidney Int Suppl: S17-26.
45. Kalyanaraman B (2013) Teaching the basics of redox biology to medical and graduate students: Oxidants, antioxidants and disease mechanisms. Redox Biol 1: 244-257.
46. Ruiz-Hurtado G, Condezo-Hoyos L, Pulido-Olmo H, Aranguez I, Del Carmen Gonzalez M, Arribas S, Cerezo C, Segura J, Praga M, Fernandez-Alfonso MS, Ruilope LM (2014) Development of albuminuria and enhancement of oxidative stress during chronic renin-angiotensin system suppression. J Hypertens 32: 2082-2091; discussion 2091.
47. Drozdz D, Kwinta P, Sztefko K, Kordon Z, Drozdz T, Latka M, Miklaszewska M, Zachwieja K, Rudzinski A, Pietrzyk JA (2016) Oxidative Stress Biomarkers and Left Ventricular Hypertrophy in Children with Chronic Kidney Disease. Oxid Med Cell Longev 2016: 7520231.
48. Arsov S, Graaff R, van Oeveren W, Stegmayr B, Sikole A, Rakhorst G, Smit AJ (2014) Advanced glycation end-products and skin autofluorescence in end-stage renal disease: a review. Clin Chem Lab Med 52: 11-20.
49. Mori T, Ogawa S, Cowely AW, Jr., Ito S (2012) Role of renal medullary oxidative and/or carbonyl stress in salt-sensitive hypertension and diabetes. Clin Exp Pharmacol Physiol 39: 125-131.

50. Suvakov S, Damjanovic T, Stefanovic A, Pekmezovic T, Savic-Radojevic A, Pljesa-Ercegovac M, Matic M, Djukic T, Coric V, Jakovljevic J, Ivanisevic J, Pljesa S, Jelic-Ivanovic Z, Mimic-Oka J, Dimkovic N, Simic T (2013) Glutathione S-transferase A1, M1, P1 and T1 null or low-activity genotypes are associated with enhanced oxidative damage among haemodialysis patients. Nephrol Dial Transplant 28: 202-212.

51. Adema AY, van Ittersum FJ, Hoenderop JG, de Borst MH, Nanayakkara PW, Ter Wee PM, Heijboer AC, Vervloet MG, consortium N (2016) Reduction of Oxidative Stress in Chronic Kidney Disease Does Not Increase Circulating alpha-Klotho Concentrations. PLoS One 11: e0144121.

52. Boudouris G, Verginadis, II, Simos YV, Zouridakis A, Ragos V, Karkabounas S, Evangelou AM (2013) Oxidative stress in patients treated with continuous ambulatory peritoneal dialysis (CAPD) and the significant role of vitamin C and E supplementation. Int Urol Nephrol 45: 1137-1144.

53. Aveles PR, Criminacio CR, Goncalves S, Bignelli AT, Claro LM, Siqueira SS, Nakao LS, Pecoits-Filho R (2010) Association between biomarkers of carbonyl stress with increased systemic inflammatory response in different stages of chronic kidney disease and after renal transplantation. Nephron Clin Pract 116: c294-299.

54. Kalousova M, Zima T, Tesar V, Dusilova-Sulkova S, Skrha J (2005) Advanced glycoxidation end products in chronic diseases-clinical chemistry and genetic background. Mutat Res 579: 37-46.

55. Ohno Y, Kanno Y, Takenaka T (2016) Central blood pressure and chronic kidney disease. World J Nephrol 5: 90-100.

56. Rubattu S, Mennuni S, Testa M, Mennuni M, Pierelli G, Pagliaro B, Gabriele E, Coluccia R, Autore C, Volpe M (2013) Pathogenesis of chronic cardiorenal syndrome: is there a role for oxidative stress? Int J Mol Sci 14: 23011-23032.

57. Himmelfarb J, Stenvinkel P, Ikizler TA, Hakim RM (2002) The elephant in uremia: oxidant stress as a unifying concept of cardiovascular disease in uremia. Kidney Int 62: 1524-1538.

58. Tampe B, Zeisberg M (2014) Contribution of genetics and epigenetics to progression of kidney fibrosis. Nephrol Dial Transplant 29 Suppl 4: iv72-79.

59. Mennuni S, Rubattu S, Pierelli G, Tocci G, Fofi C, Volpe M (2014) Hypertension and kidneys: unraveling complex molecular mechanisms underlying hypertensive renal damage. J Hum Hypertens 28: 74-79.

60. Schulz A, Kreutz R (2012) Mapping genetic determinants of kidney damage in rat models. Hypertens Res 35: 675-694.

61. Bonomo JA, Guan M, Ng MC, Palmer ND, Hicks PJ, Keaton JM, Lea JP, Langefeld CD, Freedman BI, Bowden DW (2014) The ras responsive transcription factor RREB1 is a novel candidate gene for type 2 diabetes associated end-stage kidney disease. Hum Mol Genet 23: 6441-6447.

62. Kao WH, Klag MJ, Meoni LA, Reich D, Berthier-Schaad Y, Li M, Coresh J, Patterson N, Tandon A, Powe NR, Fink NE, Sadler JH, Weir MR, Abboud HE, Adler SG, Divers J, Iyengar SK, Freedman BI, Kimmel PL, Knowler WC, Kohn OF, Kramp K, Leehey DJ, Nicholas SB, Pahl MV, Schelling JR, Sedor JR, Thornley-Brown D, Winkler CA, Smith MW, Parekh RS, Family Investigation of N, Diabetes Research G (2008) MYH9 is associated with nondiabetic end-stage renal disease in African Americans. Nat Genet 40: 1185-1192.

63. Lumbers ER, Pringle KG, Wang Y, Gibson KJ (2013) The renin-angiotensin system from conception to old age: the good, the bad and the ugly. Clin Exp Pharmacol Physiol 40: 743-752.

64. Kestila M, Lenkkeri U, Mannikko M, Lamerdin J, McCready P, Putaala H, Ruotsalainen V, Morita T, Nissinen M, Herva R, Kashtan CE, Peltonen L, Holmberg C, Olsen A, Tryggvason K (1998) Positionally cloned gene for a novel glomerular protein--nephrin--is mutated in congenital nephrotic syndrome. Mol Cell 1: 575-582.

65. Zhang SY, Marlier A, Gribouval O, Gilbert T, Heidet L, Antignac C, Gubler MC (2004) In vivo expression of podocyte slit diaphragm-associated proteins in nephrotic patients with NPHS2 mutation. Kidney Int 66: 945-954.

66. Zeisberg M, Neilson EG (2010) Mechanisms of tubulointerstitial fibrosis. J Am Soc Nephrol 21: 1819-1834.

67. Hsu CC, Bray MS, Kao WH, Pankow JS, Boerwinkle E, Coresh J (2006) Genetic variation of the renin-angiotensin system and chronic kidney disease progression in black individuals in the atherosclerosis risk in communities study. J Am Soc Nephrol 17: 504-512.

68. Jimenez-Sousa MA, Fernandez-Rodriguez A, Heredia M, Tamayo E, Guzman-Fulgencio M, Lajo C, Lopez E, Gomez-Herreras JI, Bustamante J, Bermejo-Martin JF, Resino S (2012) Genetic polymorphisms located in TGFB1, AGTR1, and VEGFA genes are associated to chronic renal allograft dysfunction. Cytokine 58: 321-326.

69. Zaffanello M, Tardivo S, Cataldi L, Fanos V, Biban P, Malerba G (2011) Genetic susceptibility to renal scar formation after urinary tract infection: a systematic review and meta-analysis of candidate gene polymorphisms. Pediatr Nephrol 26: 1017-1029.

70. Ma LJ, Fogo AB (2003) Model of robust induction of glomerulosclerosis in mice: importance of genetic background. Kidney Int 64: 350-355.

71. Leelahavanichkul A, Yan Q, Hu X, Eisner C, Huang Y, Chen R, Mizel D, Zhou H, Wright EC, Kopp JB, Schnermann J, Yuen PS, Star RA (2010) Angiotensin II overcomes strain-dependent resistance of rapid CKD progression in a new remnant kidney mouse model. Kidney Int 78: 1136-1153.

72. Lee VW, Harris DC (2011) Adriamycin nephropathy: a model of focal segmental glomerulosclerosis. Nephrology (Carlton) 16: 30-38.

73. Tesch GH, Nikolic-Paterson DJ (2006) Recent insights into experimental mouse models of diabetic nephropathy. Nephron Exp Nephrol 104: e57-62.

74. Lee TN, Alborn WE, Knierman MD, Konrad RJ (2006) The diabetogenic antibiotic streptozotocin modifies the tryptic digest pattern for peptides of the enzyme O-GlcNAc-selective N-acetyl-beta-d-glucosaminidase that contain amino acid residues essential for enzymatic activity. Biochem Pharmacol 72: 710-718.

75. Tesch GH, Allen TJ (2007) Rodent models of streptozotocin-induced diabetic nephropathy. Nephrology (Carlton) 12: 261-266.

76. Breyer MD, Bottinger E, Brosius FC, 3rd, Coffman TM, Harris RC, Heilig CW, Sharma K, Amdcc (2005) Mouse models of diabetic nephropathy. J Am Soc Nephrol 16: 27-45.

77. Candido R, Jandeleit-Dahm KA, Cao Z, Nesteroff SP, Burns WC, Twigg SM, Dilley RJ, Cooper ME, Allen TJ (2002) Prevention of accelerated atherosclerosis by angiotensin-converting enzyme inhibition in diabetic apolipoprotein E-deficient mice. Circulation 106: 246-253.

78. Like AA, Rossini AA (1976) Streptozotocin-induced pancreatic insulitis: new model of diabetes mellitus. Science 193: 415-417.

79. Ma G, Allen TJ, Cooper ME, Cao Z (2004) Calcium channel blockers, either amlodipine or mibefradil, ameliorate renal injury in experimental diabetes. Kidney Int 66: 1090-1098.

80. Brosius FC, 3rd, Alpers CE, Bottinger EP, Breyer MD, Coffman TM, Gurley SB, Harris RC, Kakoki M, Kretzler M, Leiter EH, Levi M, McIndoe RA, Sharma K, Smithies O, Susztak K, Takahashi N, Takahashi T, Animal Models of Diabetic Complications C (2009) Mouse models of diabetic nephropathy. J Am Soc Nephrol 20: 2503-2512.

81. Betz B, Conway BR (2014) Recent advances in animal models of diabetic nephropathy. Nephron Exp Nephrol 126: 191-195.

82. Zhu C, Xuan X, Che R, Ding G, Zhao M, Bai M, Jia Z, Huang S, Zhang A (2014) Dysfunction of the PGC-1alpha-mitochondria axis confers adriamycin-induced podocyte injury. Am J Physiol Renal Physiol 306: F1410-1417.

83. De Boer E, Navis G, Tiebosch AT, De Jong PE, De Zeeuw D (1999) Systemic factors are involved in the pathogenesis of proteinuria-induced glomerulosclerosis in adriamycin nephrotic rats. J Am Soc Nephrol 10: 2359-2366.

84. Fukuda F, Kitada M, Horie T, Awazu S (1992) Evaluation of adriamycin-induced lipid peroxidation. Biochem Pharmacol 44: 755-760.

85. Barbey MM, Fels LM, Soose M, Poelstra K, Gwinner W, Bakker W, Stolte H (1989) Adriamycin affects glomerular renal function: evidence for the involvement of oxygen radicals. Free Radic Res Commun 7: 195-203.

86. Guo J, Ananthakrishnan R, Qu W, Lu Y, Reiniger N, Zeng S, Ma W, Rosario R, Yan SF, Ramasamy R, D'Agati V, Schmidt AM (2008) RAGE mediates podocyte injury in adriamycin-induced glomerulosclerosis. J Am Soc Nephrol 19: 961-972.

87. Mingyan E, Hongli L, Shufeng L, Bo Y (2008) Effects of pyrrolidine dithiocarbamate on antioxidant enzymes in cardiomyopathy induced by adriamycin in rats. Cardiology 111: 119-125.

88. Su YW, Liang C, Jin HF, Tang XY, Han W, Chai LJ, Zhang CY, Geng B, Tang CS, Du JB (2009) Hydrogen sulfide regulates cardiac function and structure in adriamycin-induced cardiomyopathy. Circ J 73: 741-749.

89. Johansen PB (1981) Doxorubicin pharmacokinetics after intravenous and intraperitoneal administration in the nude mouse. Cancer Chemother Pharmacol 5: 267-270.

90. Fujimura T, Yamagishi S, Ueda S, Fukami K, Shibata R, Matsumoto Y, Kaida Y, Hayashida A, Koike K, Matsui T, Nakamura K, Okuda S (2009) Administration of pigment epithelium-derived factor (PEDF) reduces proteinuria by suppressing decreased nephrin and increased VEGF expression in the glomeruli of adriamycin-injected rats. Nephrol Dial Transplant 24: 1397-1406.

91. Ramadan R, Faour D, Awad H, Khateeb E, Cohen R, Yahia A, Torgovicky R, Cohen R, Lazari D, Kawachi H, Abassi Z (2012) Early treatment with everolimus exerts nephroprotective effect in rats with adriamycin-induced nephrotic syndrome. Nephrol Dial Transplant 27: 2231-2241.

92. Fan Q, Xing Y, Ding J, Guan N (2009) Reduction in VEGF protein and phosphorylated nephrin associated with proteinuria in adriamycin nephropathy rats. Nephron Exp Nephrol 111: e92-e102.

93. Mahajan D, Wang Y, Qin X, Wang Y, Zheng G, Wang YM, Alexander SI, Harris DC (2006) CD4+CD25+ regulatory T cells protect against injury in an innate murine model of chronic kidney disease. J Am Soc Nephrol 17: 2731-2741.

94. Wu H, Wang Y, Tay YC, Zheng G, Zhang C, Alexander SI, Harris DC (2005) DNA vaccination with naked DNA encoding MCP-1 and RANTES protects against renal injury in adriamycin nephropathy. Kidney Int 67: 2178-2186.

95. Liu S, Jia Z, Zhou L, Liu Y, Ling H, Zhou SF, Zhang A, Du Y, Guan G, Yang T (2013) Nitro-oleic acid protects against adriamycin-induced nephropathy in mice. Am J Physiol Renal Physiol 305: F1533-1541.

96. Kokeny G, Nemeth Z, Godo M, Hamar P (2010) The Rowett rat strain is resistant to renal fibrosis. Nephrol Dial Transplant 25: 1458-1462.

97. Wang B, Chandrasekera PC, Pippin JJ (2014) Leptin- and leptin receptor-deficient rodent models: relevance for human type 2 diabetes. Curr Diabetes Rev 10: 131-145.

98. Orlando RA, Takeda T, Zak B, Schmieder S, Benoit VM, McQuistan T, Furthmayr H, Farquhar MG (2001) The glomerular epithelial cell anti-adhesin podocalyxin associates with the actin cytoskeleton through interactions with ezrin. J Am Soc Nephrol 12: 1589-1598.

99. Ohman T, Lietzen N, Valimaki E, Melchjorsen J, Matikainen S, Nyman TA (2010) Cytosolic RNA recognition pathway activates 14-3-3 protein mediated signaling and caspase-dependent disruption of cytokeratin network in human keratinocytes. J Proteome Res 9: 1549-1564.

100. Lehtonen S, Tienari J, Londesborough A, Pirvola U, Ora A, Reima I, Lehtonen E (2008) CD2-associated protein is widely expressed and differentially regulated during embryonic development. Differentiation 76: 506-517.

101. Lehtonen S, Lehtonen E, Kudlicka K, Holthofer H, Farquhar MG (2004) Nephrin forms a complex with adherens junction proteins and CASK in podocytes and in Madin-Darby canine kidney cells expressing nephrin. Am J Pathol 165: 923-936.

102. Wasik AA, Polianskyte-Prause Z, Dong MQ, Shaw AS, Yates JR, 3rd, Farquhar MG, Lehtonen S (2012) Septin 7 forms a complex with CD2AP and nephrin and regulates glucose transporter trafficking. Mol Biol Cell 23: 3370-3379.

103. Hamar P, Liptak P, Heemann U, Ivanyi B (2005) Ultrastructural analysis of the Fisher to Lewis rat model of chronic allograft nephropathy. Transpl Int 18: 863-870.

104. el Nahas AM, Zoob SN, Evans DJ, Rees AJ (1987) Chronic renal failure after nephrotoxic nephritis in rats: contributions to progression. Kidney Int 32: 173-180.

105. Hamar P, Kokeny G, Liptak P, Krtil J, Adamczak M, Amann K, Ritz E, Gross ML (2007) The combination of ACE inhibition plus sympathetic denervation is superior to ACE inhibitor monotherapy in the rat renal ablation model. Nephron Exp Nephrol 105: e124-136.

106. Lattouf R, Younes R, Lutomski D, Naaman N, Godeau G, Senni K, Changotade S (2014) Picrosirius red staining: a useful tool to appraise collagen networks in normal and pathological tissues. J Histochem Cytochem 62: 751-758.

107. Romero M, Caniffi C, Bouchet G, Costa MA, Elesgaray R, Arranz C, Tomat AL (2015) Chronic treatment with atrial natriuretic peptide in spontaneously hypertensive rats: beneficial renal effects and sex differences. PLoS One 10: e0120362.

108. Fang L, Radovits T, Szabo G, Mozes MM, Rosivall L, Kokeny G (2013) Selective phosphodiesterase-5 (PDE-5) inhibitor vardenafil ameliorates renal damage in type 1 diabetic rats by restoring cyclic 3',5' guanosine monophosphate (cGMP) level in podocytes. Nephrol Dial Transplant 28: 1751-1761.

109. Livak KJ, Schmittgen TD (2001) Analysis of relative gene expression data using real-time quantitative PCR and the 2(-Delta Delta C(T)) Method. Methods 25: 402-408.

110. Bohling T, Turunen O, Jaaskelainen J, Carpen O, Sainio M, Wahlstrom T, Vaheri A, Haltia M (1996) Ezrin expression in stromal cells of capillary hemangioblastoma. An immunohistochemical survey of brain tumors. Am J Pathol 148: 367-373.

111. Fang J, Wei H, Sun Y, Zhang X, Liu W, Chang Q, Wang R, Gong Y (2013) Regulation of podocalyxin expression in the kidney of streptozotocin-induced diabetic rats with Chinese herbs (Yishen capsule). BMC Complement Altern Med 13: 76.

112. Chua SC, Jr., Chung WK, Wu-Peng XS, Zhang Y, Liu SM, Tartaglia L, Leibel RL (1996) Phenotypes of mouse diabetes and rat fatty due to mutations in the OB (leptin) receptor. Science 271: 994-996.

113. Coimbra TM, Janssen U, Grone HJ, Ostendorf T, Kunter U, Schmidt H, Brabant G, Floege J (2000) Early events leading to renal injury in obese Zucker (fatty) rats with type II diabetes. Kidney Int 57: 167-182.

114. Ma H, Wu Y, Zhang W, Dai Y, Li F, Xu Y, Wang Y, Tu H, Li W, Zhang X (2013) The effect of mesenchymal stromal cells on doxorubicin-induced nephropathy in rats. Cytotherapy 15: 703-711.

115. Song J, Knepper MA, Verbalis JG, Ecelbarger CA (2003) Increased renal ENaC subunit and sodium transporter abundances in streptozotocin-induced type 1 diabetes. Am J Physiol Renal Physiol 285: F1125-1137.

116. Hwang HJ, Baek YM, Kim SW, Kumar GS, Cho EJ, Oh JY, Yun JW (2007) Differential expression of kidney proteins in streptozotocin-induced diabetic rats in response to hypoglycemic fungal polysaccharides. J Microbiol Biotechnol 17: 2005-2017.

117. Fievet BT, Gautreau A, Roy C, Del Maestro L, Mangeat P, Louvard D, Arpin M (2004) Phosphoinositide binding and phosphorylation act sequentially in the activation mechanism of ezrin. J Cell Biol 164: 653-659.

118. Chun KH, Choi KD, Lee DH, Jung Y, Henry RR, Ciaraldi TP, Kim YB (2011) In vivo activation of ROCK1 by insulin is impaired in skeletal muscle of humans with type 2 diabetes. Am J Physiol Endocrinol Metab 300: E536-542.

119. Zheng Z, Pavlidis P, Chua S, D'Agati VD, Gharavi AG (2006) An ancestral haplotype defines susceptibility to doxorubicin nephropathy in the laboratory mouse. J Am Soc Nephrol 17: 1796-1800.

120. de Mik SM, Hoogduijn MJ, de Bruin RW, Dor FJ (2013) Pathophysiology and treatment of focal segmental glomerulosclerosis: the role of animal models. BMC Nephrol 14: 74.

121. Bertani T, Rocchi G, Sacchi G, Mecca G, Remuzzi G (1986) Adriamycin-induced glomerulosclerosis in the rat. Am J Kidney Dis 7: 12-19.

122. Otaki Y, Miyauchi N, Higa M, Takada A, Kuroda T, Gejyo F, Shimizu F, Kawachi H (2008) Dissociation of NEPH1 from nephrin is involved in development of a rat model of focal segmental glomerulosclerosis. Am J Physiol Renal Physiol 295: F1376-1387.

123. Jeansson M, Bjorck K, Tenstad O, Haraldsson B (2009) Adriamycin alters glomerular endothelium to induce proteinuria. J Am Soc Nephrol 20: 114-122.

124. (2014) Charles River Laboratories: RNU rat. Available: http://wwwcrivercom/products-services/basic-research/find-a-model/rnu-rat.

125. Pettersen JC, Morrissey RL, Saunders DR, Pavkov KL, Luempert LG, 3rd, Turnier JC, Matheson DW, Schwartz DR (1996) A 2-year comparison study of Crl:CD BR and Hsd:Sprague-Dawley SD rats. Fundam Appl Toxicol 33: 196-211.

126. Zou MS, Yu J, Nie GM, He WS, Luo LM, Xu HT (2010) 1, 25-dihydroxyvitamin D3 decreases adriamycin-induced podocyte apoptosis and loss. Int J Med Sci 7: 290-299.

127. Machado JR, Rocha LP, Neves PD, Cobo Ede C, Silva MV, Castellano LR, Correa RR, Reis MA (2012) An overview of molecular mechanism of nephrotic syndrome. Int J Nephrol 2012: 937623.

128. Gross ML, Hanke W, Koch A, Ziebart H, Amann K, Ritz E (2002) Intraperitoneal protein injection in the axolotl: the amphibian kidney as a novel model to study tubulointerstitial activation. Kidney Int 62: 51-59.

129. Zoja C, Abbate M, Remuzzi G (2014) Progression of renal injury toward interstitial inflammation and glomerular sclerosis is dependent on abnormal protein filtration. Nephrol Dial Transplant.

130. Cianciolo R, Yoon L, Krull D, Stokes A, Rodriguez A, Jordan H, Cooper D, Falls JG, Cullen J, Kimbrough C, Berridge B (2013) Gene expression analysis and urinary biomarker assays reveal activation of tubulointerstitial injury pathways in a rodent model of chronic proteinuria (Doxorubicin nephropathy). Nephron Exp Nephrol 124: 1-10.

131. Mishra J, Ma Q, Prada A, Mitsnefes M, Zahedi K, Yang J, Barasch J, Devarajan P (2003) Identification of neutrophil gelatinase-associated lipocalin as a novel early urinary biomarker for ischemic renal injury. J Am Soc Nephrol 14: 2534-2543.

132. Mishra J, Dent C, Tarabishi R, Mitsnefes MM, Ma Q, Kelly C, Ruff SM, Zahedi K, Shao M, Bean J, Mori K, Barasch J, Devarajan P (2005) Neutrophil gelatinase-associated lipocalin (NGAL) as a biomarker for acute renal injury after cardiac surgery. Lancet 365: 1231-1238.

133. Entin-Meer M, Ben-Shoshan J, Maysel-Auslender S, Levy R, Goryainov P, Schwartz I, Barshack I, Avivi C, Sharir R, Keren G (2012) Accelerated renal fibrosis in cardiorenal syndrome is associated with long-term increase in urine neutrophil gelatinase-associated lipocalin levels. Am J Nephrol 36: 190-200.

134. Lan HY (2011) Diverse roles of TGF-beta/Smads in renal fibrosis and inflammation. Int J Biol Sci 7: 1056-1067.

135. Yanagita M (2012) Inhibitors/antagonists of TGF-beta system in kidney fibrosis. Nephrol Dial Transplant 27: 3686-3691.

136. Ruster C, Wolf G (2011) Angiotensin II as a morphogenic cytokine stimulating renal fibrogenesis. J Am Soc Nephrol 22: 1189-1199.

137. Qin XJ, He W, Hai CX, Liang X, Liu R (2008) Protection of multiple antioxidants Chinese herbal medicine on the oxidative stress induced by adriamycin chemotherapy. J Appl Toxicol 28: 271-282.

138. Morgan WA, Kaler B, Bach PH (1998) The role of reactive oxygen species in adriamycin and menadione-induced glomerular toxicity. Toxicol Lett 94: 209-215.

139. Sharkey LC, Radin MJ, Heller L, Rogers LK, Tobias A, Matise I, Wang Q, Apple FS, McCune SA (2013) Differential cardiotoxicity in response to chronic doxorubicin treatment in male spontaneous hypertension-heart failure (SHHF), spontaneously hypertensive (SHR), and Wistar Kyoto (WKY) rats. Toxicol Appl Pharmacol 273: 47-57.

140. Zheng Z, Schmidt-Ott KM, Chua S, Foster KA, Frankel RZ, Pavlidis P, Barasch J, D'Agati VD, Gharavi AG (2005) A Mendelian locus on chromosome 16 determines susceptibility to doxorubicin nephropathy in the mouse. Proc Natl Acad Sci U S A 102: 2502-2507.

141. Papeta N, Zheng Z, Schon EA, Brosel S, Altintas MM, Nasr SH, Reiser J, D'Agati VD, Gharavi AG (2010) Prkdc participates in mitochondrial genome maintenance and prevents Adriamycin-induced nephropathy in mice. J Clin Invest 120: 4055-4064.

142. Mashimo T, Takizawa A, Kobayashi J, Kunihiro Y, Yoshimi K, Ishida S, Tanabe K, Yanagi A, Tachibana A, Hirose J, Yomoda J, Morimoto S, Kuramoto T, Voigt B, Watanabe T, Hiai H, Tateno C, Komatsu K, Serikawa T (2012) Generation and characterization of severe combined immunodeficiency rats. Cell Rep 2: 685-694.

143. Mori N, Matsumoto Y, Okumoto M, Suzuki N, Yamate J (2001) Variations in Prkdc encoding the catalytic subunit of DNA-dependent protein kinase (DNA-PKcs) and susceptibility to radiation-induced apoptosis and lymphomagenesis. Oncogene 20: 3609-3619.

144. Wynn TA (2008) Cellular and molecular mechanisms of fibrosis. J Pathol 214: 199-210.

145. Zhang Y, Bao S, Kuang Z, Ma Y, Hu Y, Mao Y (2014) Urotensin II promotes monocyte chemoattractant protein-1 expression in aortic adventitial fibroblasts of rat. Chin Med J (Engl) 127: 1907-1912.

146. Lee K, Won HY, Bae MA, Hong JH, Hwang ES (2011) Spontaneous and aging-dependent development of arthritis in NADPH oxidase 2 deficiency through altered differentiation of CD11b+ and Th/Treg cells. Proc Natl Acad Sci U S A 108: 9548-9553.

10. Bibliography of the candidate's publications

10.1. Publications related to the PhD thesis

Wasik AA, Koskelainen S, Hyvonen ME, Musante L, Lehtonen E, Koskenniemi K, Tienari J, Vaheri A, Kerjaschki D, Szalay C, Revesz C, Varmanen P, Nyman TA, Hamar P, Holthofer H, Lehtonen S (2014) Ezrin is down-regulated in diabetic kidney glomeruli and regulates actin reorganization and glucose uptake via GLUT1 in cultured podocytes. Am J Pathol 184: 1727-1739.
IF: 4,591

Szalay CI, Erdelyi K, Kokeny G, Lajtar E, Godo M, Revesz C, Kaucsar T, Kiss N, Sarkozy M, Csont T, Krenacs T, Szenasi G, Pacher P, Hamar P (2015) Oxidative/Nitrative Stress and Inflammation Drive Progression of Doxorubicin-Induced Renal Fibrosis in Rats as Revealed by Comparing a Normal and a Fibrosis-Resistant Rat Strain. PLoS One 10: e0127090.
IF: 3,234

10.2. Publications unrelated to the PhD thesis

Kaucsar T, Revesz C, Godo M, Krenacs T, Albert M, Szalay CI, Rosivall L, Benyo Z, Batkai S, Thum T, Szenasi G, Hamar P (2013) Activation of the miR-17 family and miR-21 during murine kidney ischemia-reperfusion injury. Nucleic Acid Ther 23: 344-354.
IF: 2,888

Kaucsar T, Bodor C, Godo M, Szalay C, Revesz C, Nemeth Z, Mozes M, Szenasi G, Rosivall L, Soti C, Hamar P (2014) LPS-induced delayed preconditioning is mediated by Hsp90 and involves the heat shock response in mouse kidney. PLoS One 9: e92004.
IF: 3,234

DOI:10.14753/SE.2018.1981

11. Acknowledgements

First and foremost I would like to thank my supervisor, **Dr. Péter Hamar** for his efforts in teaching and supporting me during my PhD studies.

I am indebted to all my colleagues from the Institute of Pathophysiology: **Prof. Dr. László Rosivall**, Head of the Basic Medicine Doctoral School for the opportunity to carry out my PhD studies; **Dr. Gábor Szénási** for his continuous guidance; **Mária Godó**, **Dr. Tamás Kaucsár**, **Csaba Révész**, **Ágnes Cser**, **Dr. Anna Buday**, **Dr. Gábor Kökény, Dr. Nóra É. Bukosza** and **Dr. Norbert Kiss** for their kind help in the experiments and for teaching numerous methods. I want to express my gratitude to **Dr. Miklós Mózes**, whose comments were especially helpful to complete this thesis.

I would also like to thank **Sanna Lehtonen**, **Anita A. Wasik** and **Niina Rouho** and all the members of the Department of Pathology of the Haartman Institute (University of Helsinki, Finland) for the possibility to be involved in their research. Without their help, this thesis would not have been possible.

I would like to offer my special thanks to **Dr. Pál Pacher** and **Katalin Erdélyi** and all the members of the Laboratory of Cardiovascular Physiology and Tissue Injury (National Institute of Health, Bethesda, Maryland, USA) for all their technical and financial support.

Deepest gratitude to **Dr. Tibor Krenács** and **Dr. Nóra Meggyesházi** from the 1st Department of Pathology and Experimental Cancer Research (Semmelweis University, Hungary), who co-operated especially with the immunohistological examinations.

I would like to show my appreciation to **Dr. Márta Sárközy** and **Dr. Tamás Csont** from the Department of Biochemistry (University of Szeged, Hungary); for all their contribution to this thesis.

I also wish to thank **Dr. Róbert Glávits**, for his tutoring and introducing me to the interesting world of histopathology.

Furthermore, I am very grateful to my parents and my siblings for trusting me and for the unconditional support and encouragement during my professional trainings.

Research in this thesis was supported by the Hungarian Scientific Research Fund (OTKA-ANN(FWF) 110810 and OTKA-SNN 114619), and by the Intramural Research Program of NIAAA/NIH.